# Spatial and seasonal variations of aerosols over China from two decades of multi-satellite observations. Part 2: AOD time series for 1995-2017 combined from ATSR ADV and MODIS C6.1 and AOD tendencies estimation

Larisa Sogacheva[1*], Edith Rodriguez[1], Pekka Kolmonen[1], Timo H. Virtanen[1], Giulia Saponaro[1], Gerrit de Leeuw[1], Aristeidis K. Georgoulias[2], Georgia Alexandri[2], Konstantinos Kourtidis[2] and Ronald J. van der A[3]

[1]Finnish Meteorological Institute(FMI), Climate Research Programme, Helsinki, Finland
[2]Laboratory of Atmospheric Pollution and Pollution Control Engineering of Atmospheric Pollutants, Department of Environmental Engineering, Democritus University of Thrace, Xanthi, Greece
[3] Royal Netherlands Meteorological Institute (KNMI), De Bilt, Netherlands

* Correspondence to: Larisa Sogacheva (larisa.sogacheva@fmi.fi)

**Abstract**

Understanding long-term variations in aerosol loading is essential for evaluating the health and climate effects of airborne particulates as well as the effectiveness of the pollution control policies. The expected satellite lifetime is about 10 to 15 years. To study the variations of atmospheric constituents over longer periods, the information from different satellites should be utilized. Here we introduce a method to construct a combined annual and seasonal long time series of AOD at 550 nm using the Along-Track Scanning Radiometers (ATSR: ATSR-2 and AATSR) and MODerate resolution Imaging Spectroradiometer Terra (MODIS/Terra), which together cover the 1995-2017 period. The long-term (1995-2017) combined AOD time series are presented for all of mainland China, for southeastern (SE) China and for 10 selected regions in China. Linear regression was applied to the combined AOD time series constructed for individual L3 (1°x1°) pixels to estimate the AOD tendencies for two periods: 1995-2006 (P1) and 2011-2017 (P2), as regarding the changes in the emission reduction policies in China.

During P1, the annually averaged AOD increased with 0.006 (or 2% of the AOD averaged over the corresponding period) per year across all of mainland China, reflecting increasing emissions due to rapid economic development. In SE China, the annual AOD positive tendency in 1995-2006 was 0.014 (3%) per year, reaching maxima (0.020, or 4%, per year) in Shanghai and the Pearl River Delta regions. After 2011, during P2, AOD tendencies reversed across most of China with annually averaged AOD decrease by -0.015 (-6%) per year in response to effective reduction in anthropogenic emissions of primary aerosols, $SO_2$ and NOx. The strongest AOD decrease is observed in the Chengdu (-0.045, or -8%, per year) and Zhengzhou (-0.046, or -9%, per year) areas, while over the North China plane and coastal areas the AOD decrease was lower than -0.03 (approximately -6%), per year. In the less populated areas, the AOD decrease was small.

The AOD tendency vary by both season and region. The increase in the annually averaged AOD during P1 was mainly due to increase in summer and autumn in SE China (0.020, or 4%, and 0.016, or 4%, per year, respectively), while during winter and spring the AOD actually decreased over most of China. The AOD negative tendencies in 2011-2017 were larger in summer than in other seasons over China (ca. -0.021, or -7%, per year) and over SE China (ca. -0.048, or -9%, per year).

The long-term AOD variations presented here show that the changes in the emission regulations policy in China during 1995-2017 result in a gradual decrease of the AOD after 2011 with an average reduction of 30%-50% between 2011 and 2017. The effect is more visible in the highly populated and industrialized regions in SE China, as expected.

## 1 Introduction

Atmospheric aerosols play an important role in climate change through direct and indirect processes. In order to evaluate the effects of aerosols on climate, it is necessary to study their spatial and temporal distributions. Understanding the long-term changes and the trend in AOD on the Earth, especially in the developing countries like China, becomes increasingly essential for accurate assessment the radiative forcing effects on climate (Li et al., 2013). The rapid development of industry, traffic and urbanization, the combustion of fossil fuel, the emissions of industrial fumes and contaminated gas lead to a significant increase of atmospheric aerosols, which do not only affect climate, but also constitute a threat to human health (Tie et al., 2009; Cao et al., 2017). It is critical for environmental and epidemiological studies to accurately investigate the fine-scale spatial and temporal changes in aerosol concentrations regarding the industrialization and urbanization (Streets et al., 2009; Kanakidou, 2014).

The air pollution in China is severe (Bouarar et al., 2017), widely distributed, and the atmospheric chemical reactions are complex (Kulmala et al., 2015). The strong economic growth in China (World Bank, 2017; Morrison, 2018) has significantly raised the living standards (Zhang K., 2017), but it has also brought serious environmental damage and degradation (Tang et al., 2015). In 1970–1990, the dominant contributing sources were big and small coal burning stoves widely used in power plants, industry, utilities and households (Jin et al., 2016). Coal smoke mainly contains sulphuric acid ($SO_2$), total suspended particle matter (TSP), but also nitrogen oxides ($NO_X$) and carbon monoxide (CO), which affect air quality by atmospheric aerosol formation (Siihto et al., 2006; Fuzzy et al., 2015; Sarrafzadeh et al., 2016; Nzihou and Stanmore, 2015). Other sources, such as dust from construction sites, are mainly consisting of primary PMs. During the period from 1990 to 2000, the growing number of vehicles, mainly in megacities contributed a lot to the increase in $NO_x$ and volatile organic compounds (VOCs). From 2000 to the present, the anthropogenic air pollution is ingrained in the megacities and spreading to the regional level (Jin et al., 2016). However, national and regional plans, environmental laws, rules and standards exist in China, which are revised with the Five-Years-Plans, which are series of social and economic development initiatives (Jin et al., 2016).

The further urbanization is a consequence of a growing industry. During the 1978–2016 period, more than 550 million migrants moved to China's cities, resulting in a large rise of urban population from 18 to 57% (Zhang, 2017). The coastal regions where manufacturing and services are better developed, especially big cities, were the principal destinations (Chan, 2012). During the last two decades, a strong population inflow to eastern China has been reported (Ma and Chen, 2012; Center for International Earth

Science Information Network - CIESIN - Columbia University, 2017). The population in the North China Plane, the Yangtze River Delta and the Pearl River Delta was steadily increasing mainly due to the growth of large cities, or metropolises (Fig. 1) on account of migration from the less industrialised areas (see also Kourtidis et al., 2015; Stathopoulos et al., 2017). The population density has increased in the Beijing-Tianjin-Hebei area, Shanghai, Xiamen and Guangzhou, by more than 200% in 2000-2015 while in Wuhan, Chengdu and Zhengzhou the population has grown by nearly 50%. Such strong population growth has resulted in the fast urbanization and the further industrialisation and infrastructure development in those regions.

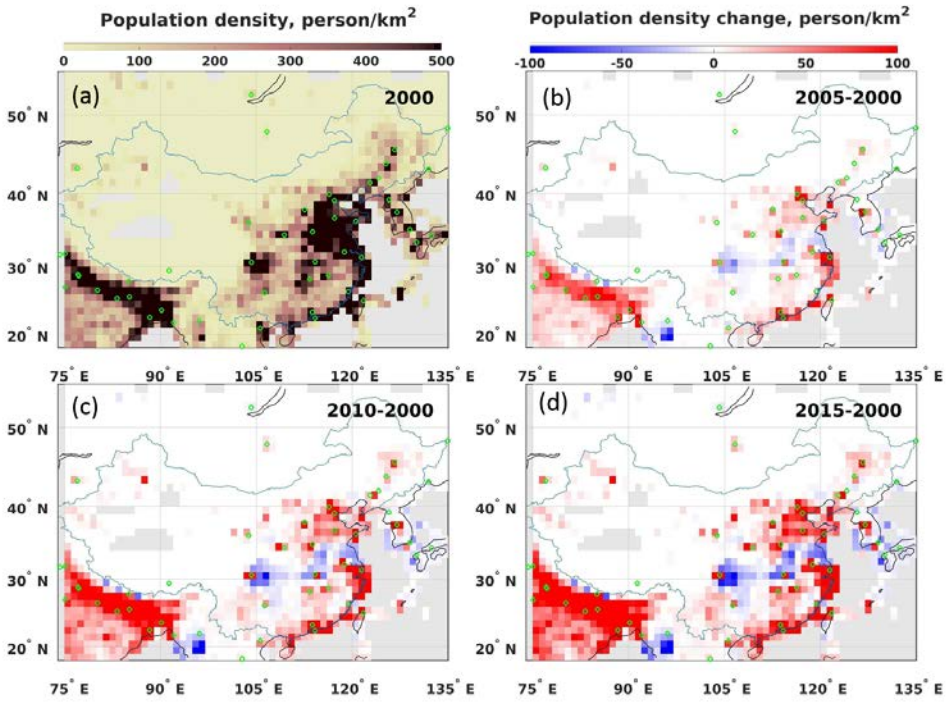


**Figure 1. The population density in China (doi: 10.7927/H4DZ068D) in 2000 (a) and the population density change in 2005 (b), 2010 (c), 2015 (d) compared with 2000. Megacities are marked with green circles.**

Due to the sparse surface network in China and limited data availability, the satellite remote sensing is increasing used to study the long-term changes in aerosol properties over China. Satellite remote sensing is a rapidly developing technology that may provide a good temporal sampling and a superior spatial coverage to study aerosols. The most common parameter derived from satellite observations is the Aerosol Optical Depth (AOD), which is a measure of the extinction of solar radiation at a given wavelength due to the presence of aerosols integrated over the atmospheric column. AOD is a key factor for the estimation of the aerosol concentration, the evaluation of atmospheric conditions and the effect of atmospheric aerosols on climate.

Su et al. (2010) analyzed the AOD distribution over 10 locations in East Asia using the yearly mean AOD products from POLDER (Polarization and Directionality of the Earth´s Reflectance) radiometer during the period from 2005 to 2009 and showed that the spatial distribution of fine-mode aerosols over East Asia is highly associated with human activities. Xie and Xia (2008) reported statistically increasing AOD trends in spring and summer in north China annually during the period from 1982 to 2001 using the Total Ozone Mapping Spectrometer (TOMS). They also demonstrated the increasing tendency of AOD (500 nm) from 1980 to 1991 and a reverse tendency from 1997 to 2001 in north China. Guo et al. (2012), who analyzed the AOD trends of TOMS and MODIS in China in 1982-2008, have reported similar findings. The spatial variation in AOD suggests no apparent upward trends in 1980's; since 1990, both TOMS and MODIS indicate a significant AOD increase across China (Guo et al., 2012). Seasonal patterns in the AOD regional long-term trend are revealed. As shown by Guo et al. (2011), AODs exhibit mostly similar seasonality during the period from 1980 to 2001: AOD maxima is observed in winter (except for Taklimakan Desert), in summer the AOD is higher than in autumn; while there is not such seasonality in 2000–2008. Li et al. (2014) reported opposite AOD trends in different locations in China using observations from the Aerosol Robotic Network (AERONET, Holben et al., 1998). Increasing trends in China over the last decades are revealed by Wang et al. (2017), while a few recent studies (Zhang et al., 2016; He et al., 2016; Mehta et al., 2016; Zhao et al., 2017; Zhang J. et al., 2017) showed decreasing trends in China in the last few years.

The expected satellite lifetime is about 10 to 15 years. To study the variations of atmospheric constituents over longer periods, the information from different satellites should be utilized (Weatherhad et al., 2017). Combining multiple sensors could increase the period for data availability and reduce data uncertainties (Li et al., 2016).

In this study, we introduce a method to combine seasonal and annual AOD data retrieved from the Along-Track Scanning Radiometers (ATSR-2 and AATSR, here-after referred as ATSR) and the MODerate resolution Imaging Spectroradiometer Terra (MODIS/Terra) to create multi-decadal time series covering the period from 1995 to 2017 to investigate AOD tendencies in China. The method is based on the results from the comparison between ATSR and MODIS AOD products presented in Sogacheva et al. (2018), further referred as Part 1. We also investigate whether the tendencies in AOD are related to the pollution control policies in China. In view of the spatial AOD variations across China (de Leeuw et al., 2018; Part 1, and references cited there in), we present combined AOD time series and estimate AOD tendencies for different regions in China.

The objectives of this study are: (1) to combine AATSR Dual View (ADV, Ver2.31) and MODIS/Terra collection 6.1 (C6.1) seasonal and annual aerosol data during 1995–2017 and (2) to analyze the spatial and temporal variations of the seasonally and annually averaged AOD and link the AOD tendencies to emission control policies in China.

The paper is structured as follows. The AATSR and MODIS/Terra AOD products are briefly introduced in Sect. 2, including the short description of the instruments, aerosol retrieval algorithms, datasets and validation results (for more details see Part 1). The study area is discussed in Sect. 3, where 10 selected regions are introduced. In Sect. 4, a method is presented to construct the combined from ATSR (1995-2011) and MODIS (2000-2017) seasonal and annual AOD and the AOD correction applied to ATSR and MODIS AOD is discussed (Sect. 4.1), the long-term annual and seasonal combined AOD time series are introduced (Sect. 4.2) and evaluated with the AERONET. (Sect. 4.3). In Sect. 5 we present and discuss the results for the AOD evolution over China (Sect.

5.1) and relate them to changes in the emission reduction policies (Sect. 5.2). The AOD tendencies for selected periods and regions are presented and discussed in Sect. 5.3. The main conclusions are summarised in Sect. 6.

## 2 Study area and selection of the regions

China covers a huge territory with significant regional differences (Fig. 2). Climate in China varies from subarctic (north) to subtropical (south). The west and north of the country are dominated by deserts (such as the Gobi and the Taklamakan), rolling plateaus, and towering massifs. The southern areas of the country is hilly and mountainous terrain. The eastern plains and southern coasts of the country consist of fertile lowlands and foothills. The contradictions between the economic growth and the environmental quality have varying dimensions in different regions.The largest agricultural provinces are Henan, Sichuan, Hunan, Anhui, and Jiangsu with low population growth and Shandong, Heilongjiang, and Hubei with balanced urbanization and agricultural development. Corresponding differences among regions exists by means of land urbanization (Lin et al., 2015). The highest population density is observed in the east and southeast (Fig. 1). Cities with rapid land urbanization are mainly distributed in the coastal regions and also scattered throughout the inland regions. Sparsely populated areas are provinces in the western China. Therefore, from a regional perspective, there are large differences in the levels of economic development in China and the efficiency of the SE China is far higher than that of the Central and the Western regions. Additionally, the gap between them tends to expand (Yang and Wang, 2013).

As in Part 1, in current study we focus on the entire area of mainland China, i.e., the area between 18–54º N and 73–135º E defined as 1º × 1º grid cells with retrievals over land and constrained by the borders indicated by the black line in Fig. 2. Purple lines indicate SE China, defined in this study as the over-land area between 20 º - 41 º N and 103 º – 135 º E. The numbers indicate the ten study regions. Regions 1-7 nearly cover the SE China. Region 8 covers the Taklamakan Desert, region 9 is over the Tibetan Plateau, and region 10 is over the northeast (NE) China. Note that all areas used in this study only consider the AOD over mainland China, i.e. AOD over the oceans or islands is not included.

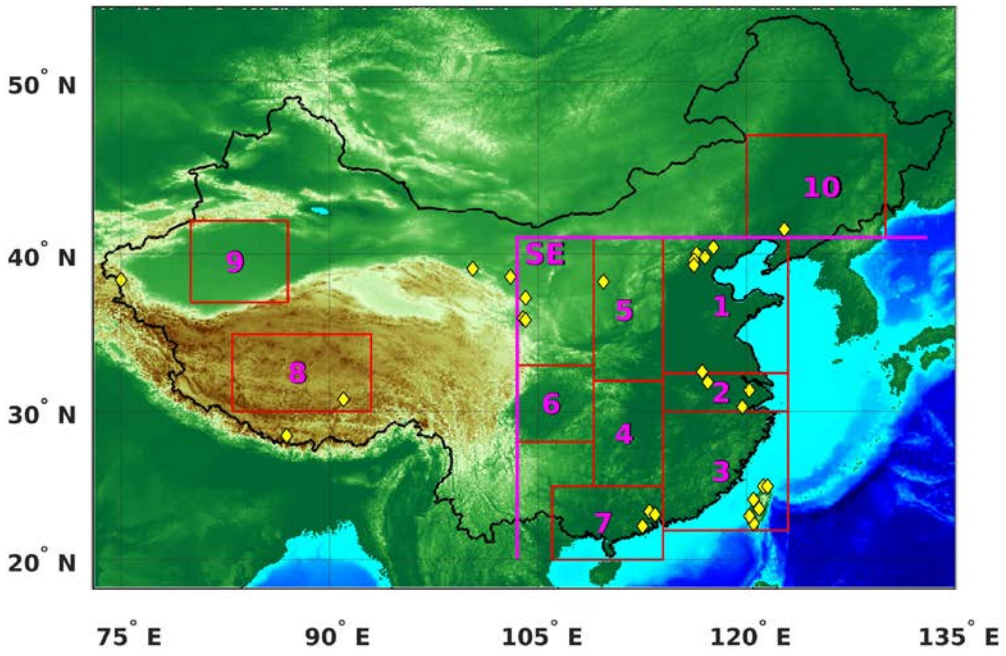


**Figure 2. Regions over mainland China (indicated with the purple numbers and red borders) selected for study of seasonal, interannual and long-term behavior of the AOD and the locations of the Aerosol Robotic Network (AERONET) sites (yellow diamonds) used in this study for validation. The black line indicates mainland China. A larger area over southeastern China is indicated by SE and purple border.**

With some deviations, the choice of the regions is similar to those in other studies (e.g., Luo et al., 2014, Wang et al., 2017). This choice covers major urban/industrial regions such as the Beijing-Tianjin-Hebei (BTH) area, the Yangtze River Delta (YRD) and the Pearl River Delta (PRD), Sichuan/Chongqing as well as cleaner regions in the northwest (region 10 in Fig. 2) and southeast (region 3). The Tibetan Plateau and the Taklamakan Desert regions, which are an important source of dust particles in China, were chosen to represent the sparsely populated and less developed, in terms of industrialization, regions.

## 3 AOD data: instrumentation, AOD retrieval algorithms and aerosol datasets

Below we briefly introduce the ATSR and MODIS instruments, AOD retrieval algorithms and the AOD datasets. For more details (e.g., difference in ATSR and MODIS AOD spatial and temporal coverage), see de Leeuw et al. (2018) and Part 1.

### 3.1 ATSR ADV

The ATSR instruments, ATSR-2 on board the European Remote Sensing satellite ERS-2 (1995-2003) and AATSR on board the environmental satellite Envisat (2002-2012), hereafter together referred as ATSR, were developed to provide high-accuracy measurements of the Sea Surface Temperature. However, they are also successfully used for atmospheric aerosol retrievals (e.g., Flowerdew and Haigh, 1996; Veefkind et al. 1998; Sayer et al., 2010; de Leeuw et al., 2015; Kolmonen et al., 2016; Popp et al., 2016). Together, these instruments provided 17 years of global data. Both satellites flew in a sun-synchronous descending orbit with a daytime equator crossing time at 10:30 (ERS-2) and 10:00 local time (Envisat). The ATSR is a dual view instrument. One view is near-nadir and the other one is at a 55$^o$ forward angle. The time between the two views is approx. 150 seconds along the track. The nominal resolution at nadir is 1x1 km$^2$ and the swath width is 512 km, which results in global coverage in 5-6 days. ATSR has three wave bands in the visible – near infrared (centred near 555 nm, 659 nm, 865 nm) and four bands in the mid- to thermal infrared (centred near 1600 nm, 3700 nm, 10850 nm, 12000 nm).

Over land, the ATSR ADV AOD retrieval algorithm uses the two ATSR views simultaneously to eliminate the contribution of land surface reflectance to the TOA radiation and retain the path radiance in cloud-free scenes (Veefkind et al., 1998, Kolmonen et al., 2016, Sogacheva et al., 2017) following Flowerdew and Haigh (1996).

ATSR-2 AOD data are available for the period from June 1995 to December 2003, with some gaps in 1995 (from January to May, globally) and 1996 (from January to June, globally), while also toward the end (approx. from autumn 2002) the data are less reliable. AATSR data are available for May 2002 - April 2012, but some data are missing in 2002 and therefore we use AATSR data only from August 2002 onward. The consistency between the ATSR-2 and AATSR datasets was discussed in Popp et al. (2016). Over China, the difference between the ADV AOD values retrieved from ATSR-2 and AATSR is small, as shown by pixel-by-pixel and monthly aggregate comparisons as well as validation results (Part 1). This allows for the combination of the ATSR-2 and AATSR AOD time series into one dataset without offset correction over China.

The L3 (averaged on a grid of 1$^o$x1$^o$) seasonal aggregates were obtained for winter (DJF), spring (MAM), summer (JJA) and autumn (SON) by averaging the L3 monthly aggregates to corresponding seasons. The annual AOD data were obtained by averaging the monthly AOD data. Hereunder, the ATSR ADV Ver. 2.31 AOD product will be referred to as ADV.

### 3.2 MODIS

The MODIS/Terra sensor (Salomonson et al., 1989) aboard NASA's Terra satellite is flying in a near-polar sun-synchronous circular orbit for more than fifteen years since December 1999. MODIS/Terra has a daytime equator crossing time at 10:30 local time (descending orbit), a viewing swath of 2330 km (cross track) and provides near-global coverage on a daily basis. Its detectors measure 36 spectral bands between 0.405 and 14.385 μm, and it acquires data at three spatial resolutions (250m, 500m, and 1000m). MODIS AOD is retrieved using two separate algorithms, Dark Target (DT) and Deep Blue (DB). In fact, two different DT algorithms are utilized, one for retrieval over land (Kaufman et al., 1997; Remer et al., 2005; Levy et al., 2013) and one for retrieval over water surfaces (Tanré et al., 1997; Remer et al., 2005, Levy et al., 2013). The DB algorithm (Hsu et al., 2004, 2013) was traditionally used

over bright surfaces where DT performance is limited (e.g. deserts, arid and semi-arid areas) and was further developed for returning aerosol measurements over all land types (Sayer et al., 2014).Hereafter, the MODIS/Terra AOD C6.1 DTDB merged AOD product will be referred to as MODIS.

### 3.3 ADV and MODIS validation results.

AOD Level 2 (L2, 0.1º x 0.1º resolution) validation with the AERONET L2.0 (quality-assured) AOD over China for ADV (de Leeuw et al., 2018) and MODIS C6.1 is discussed in detail in Part 1. The location of the AERONET stations used in this study for validation is shown in Fig.2. Note that the number of the AERONET stations is limited over north-west of China (de Leeuw et al., 2018; Part 1).Validation results are briefly summarized in this section. For all available collocations between ADV and AERONET and between MODIS and AERONET (Table 1, "All points") MODIS algorithm performs slightly better than ADV. The correlation coefficients are 0.88 for ADV and 0.92 for MODIS (note, that since MODIS has better coverage as compared to ADV (Part 1), the number of validation points for MODIS is considerably larger). Both algorithms show similar (in absolute numbers) bias, which is negative for ADV (-0.06) and positive for MODIS (0.07). AOD standard deviation (δ) and root mean square error (rms) are slightly lower for MODIS. Similar in absolute values but different in sign AOD bias was obtained also for "fine-dominated" (AOD>0.2, AE>1) and for "coarse-dominated" (AOD>0.2, AE<1) aerosol conditions (-0.11 and 0.10, for ADV and MODIS, respectively).

**Table 1. ADV and MODIS AOD validation results over China for the overlapping period 2000-2011. Statistics (number of points (N), correlation coefficient (R), bias, standard deviation (σ) and root mean square error (rms)) for all validation points, separately for "fine-dominated" (AOD>0.2, AE>1) and "coarse-dominated" (AOD>0.2, AE<1) aerosols, and collocated points (*when ADV and MODIS overpasses are within ±90min from each other and ADV, MODIS and AERONET retrieve AOD). For collocated points, statistics are aggregated also seasonally for winter (DJF), spring (MAM), summer (JJA) and autumn (SON).**

| | N | | R | | bias | | σ | | rms | |
|---|---|---|---|---|---|---|---|---|---|---|
| | **ADV** | **MOD** | **ADV** | **MOD** | **ADV** | **MOD** | **ADV** | **MOD** | **ADV** | **MOD** |
| **All points** | | | | | | | | | | |
| | 1132 | 4963 | 0.88 | 0.92 | -0.07 | 0.06 | 0.007 | 0.003 | 0.24 | 0.20 |
| e.g. fine-dominated | 482 | 1983 | 0.85 | 0.89 | -0.09 | 0.08 | 0.014 | 0.005 | 0.30 | 0.24 |
| e.g., coarse-dominated | 129 | 970 | 0.85 | 0.88 | -0.11 | 0.10 | 0.032 | 0.007 | 0.37 | 0.22 |
| **Collocated* Points:** | | | | | | | | | | |
| **All collocated points** | 255 | | 0.92 | 0.93 | -0.11 | 0.06 | 0.01 | 0.008 | 0.17 | 0.16 |
| **Collocated points, seasons:** | | | | | | | | | | |
| **DJF** | 10 | | 0.92 | 0.96 | -0.04 | -0.17 | 0.023 | 0.052 | 0.10 | 0.19 |
| **MAM** | 87 | | 0.81 | 0.81 | 0.00 | 0.13 | 0.012 | 0.013 | 0.16 | 0.14 |
| **JJA** | 73 | | 0.94 | 0.96 | -0.13 | 0.13 | 0.029 | 0.017 | 0.25 | 0.22 |
| **SON** | 85 | | 0.92 | 0.88 | -0.02 | 0.05 | 0.007 | 0.009 | 0.10 | 0.09 |

To compare the performance of the two algorithms when both ADV and MODIS retrieve AOD, we carried out the AOD validation for the cases, when the difference between ATSR and MODIS/Terra overpasses was less than 90 minutes and both ADV and MODIS have successfully retrieved AOD around AERONET (Table 1, "Collocated points"). Altogether, 255 collocations exist between ADV, MODIS and AERONET for the ATSR and MODIS/Terra overlapping period (2000-2011) over China. Validation was done for all collocated points and for each of the four seasons: DJF, MAM, JJA, and SON. For all collocated points, the correlation coefficients (R) were similar for ADV and MODIS (0.92 and 0.93, respectively), ADV was biased negatively (-0.11), while MODIS was biased positively (0.06). In winter, MODIS showed a strong negative bias in AOD (-0.17), while the correlation for MODIS was higher than for ADV (0.96 and 0.92, respectively). Note, that the number of collocated points was low (10) in winter. In spring, R was the same (0.81) for MODIS and ADV, while bias is 0 for ADV and 0.013 for MODIS. Interestingly, both MODIS and ADV showed similar tendency of underestimation of AERONET AOD for AOD >0.6 in spring. In summer, R was a bit higher for MODIS; biases for ADV and MODIS were equal in an absolute sense but opposite in sign (negative for ADV and positive for MODIS). In autumn, R was a higher for ADV (0.92 versus 0.88 for MODIS), the bias was negative for ADV (-0.02) and positive for MODIS (0.05).

In summary, MODIS showed a better performance for the "all points" selection. Similar (in absolute numbers) bias, which is negative for ADV and positive for MODIS, is considered in Sect. 4, where a method for combining the two datasets is presented. For collocated points, ADV and MODIS showed similar performance.

## 4 Long-term (1995-2017) annual and seasonal AOD time series combined from ADV and MODIS

Here we introduce a method to combine the AOD data from the ATSR (1995-2011) and MODIS/Terra (2000-2017) radiometers, which together cover the period from 1995 to 2017. The results from the comparison of the ADV and MODIS AOD datasets in Part 1 are used here to construct a combined AOD dataset. Below, some conclusions obtained in Part 1 are highlighted.

(1) Similar AOD patterns are observed by ADV and MODIS in yearly and seasonal aggregates (Part 1). However, the ADV-MODIS difference maps (Part 1, Fig. 10 (right)) show that MODIS AOD is mostly higher than that from ADV.

(2) The time series in Figs. 13 and S1-S4 (Part 1) show large differences between regions, for both sensors, while the interannual patterns in the time series are similar for both ADV and MODIS.

(3) Similar patterns exist in year-to-year ADV and MODIS annual AOD tendencies in the overlapping period (Part 1, Tab S2).

(4) ADV and MODIS validation with AERONET data (Part 1, Sect. 4) shows similar high correlation (0.88 and 0.92, respectively), while the bias is of similar magnitude but opposite in sign: positive for MODIS (0.06) and negative for ADV (-0.07). Similar in absolute values but opposite in sign AOD bias is calculated for "fine-dominated" (-0.09 and 0.08, for ADV and MODIS, respectively) and for "coarse-dominated" aerosol conditions (-0.11 and 0.10, for ADV and MODIS, respectively).

### 4.1 Method

The combined AOD ($AOD_{comb,}$) database for the period from 1995 to 2017 was compiled from AOD estimated for three periods. The first period (T1) is the pre-EOS period (1995-1999), when only ATSR was available, the second period (T2) is the ATSR and MODIS/Terra overlapping period (2000-2011) and the third (T3) is the post-ENVISAT (2012-2017) period, when only MODIS/Terra was available:

$$AOD_{comb} = [AOD_{T1},\ AOD_{T2},\ AOD_{T3}]\ . (1)$$

First, we introduce the combined AOD for the overlapping period T2, when AOD for both ADV ($AOD_{ADV}$) and MODIS ($AOD_{MOD}$) was available. AOD for each year ($AOD_{T2,y}$) is calculated as a mean of $AOD_{ADV,y}$ and $AOD_{MOD,y}$:

$$\mathrm{AOD_{T2,y}} = \frac{\mathrm{AOD_{MOD,y}+AOD_{ADV,y}}}{2}\ . (2)$$

The simple averaging was applied, since ADV and MODIS show similar biases of opposite signs (Sect. 2.3 and Part 1).

Using ADV and MODIS yearly AOD from T2, the AOD correction ($AOD_{corr}$) was calculated as the mean difference between ADV and MODIS for the overlapping period:

$$AOD_{corr} = \frac{\sum \frac{AOD_{MOD,y,} - AOD_{ADV,y}}{2}}{N}\ ,\ (3)$$

where N is the length of the overlapping period in years.

For ADV and MODIS respectively, the AOD correction was scaled by the corresponding AOD, averaged over the overlapping period:

$$\mathrm{AOD_{rel\_corr,ADV}} = \mathrm{AOD_{corr}} \Big/ \mathrm{mean(AOD_{ADV,T2})},\quad (4)$$

$$\mathrm{AOD_{rel\_corr,MOD}} = \mathrm{AOD_{corr}} \Big/ \mathrm{mean(AOD_{MOD,T2})}\ .\quad (5)$$

For T1 and T3, the AOD relative correction ($\mathrm{AOD_{rel\_corr}}$) was applied as positive correction for usually lower ADV AOD (eq. 6) and negative correction for usually higher MODIS AOD (eq. 7)

$$\mathrm{AOD_{T1,y,}} = \mathrm{AOD_{ADV,y,}}*(1 + \mathrm{AOD_{rel\_corr,ADV}})\ , (6)$$

$$\mathrm{AOD_{T3,y,}} = \mathrm{AOD_{MOD,y,}}*(1\text{-}\mathrm{AOD_{rel\_corr,MOD}})\ (7).$$

The spatial distributions of the relative correction for MODIS AOD ( $AOD_{rel\_corr,MODIS}$ ) are shown in Fig. 3 for annual and seasonal AOD aggregates. As expected, the highest AOD relative correction (30-40%) corresponds to the areas, where the agreement is lower between ADV and MODIS AOD ( Fig. 10 in Part 1), e.g., over the bright surface areas, such as Tibetan Plateau and the Taklamakan and Gobi Deserts and Harbin area. The reasons for disagreement between ADV AOD and MODIS AOD, related mostly to the coverage and validation results, is discussed in detail in Part 1 and Sect. 3.3 of the current paper. For seasonal aggregates, the highest

correction (ca 45%) is obtained over the Tibetan Plateau in autumn, when AOD is lower compared to spring and summer (Fig. 10 in Part 1). In summer, the correction is smaller, since in that season the agreement between the ADV and MODIS AOD is better than in other seasons (Fig. 10 in Part 1).Over SE China, the AOD correction is lower (between 10% and 20% of AOD). The ADV AOD relative correction shows similar spatial patterns and therefore is not discussed here.

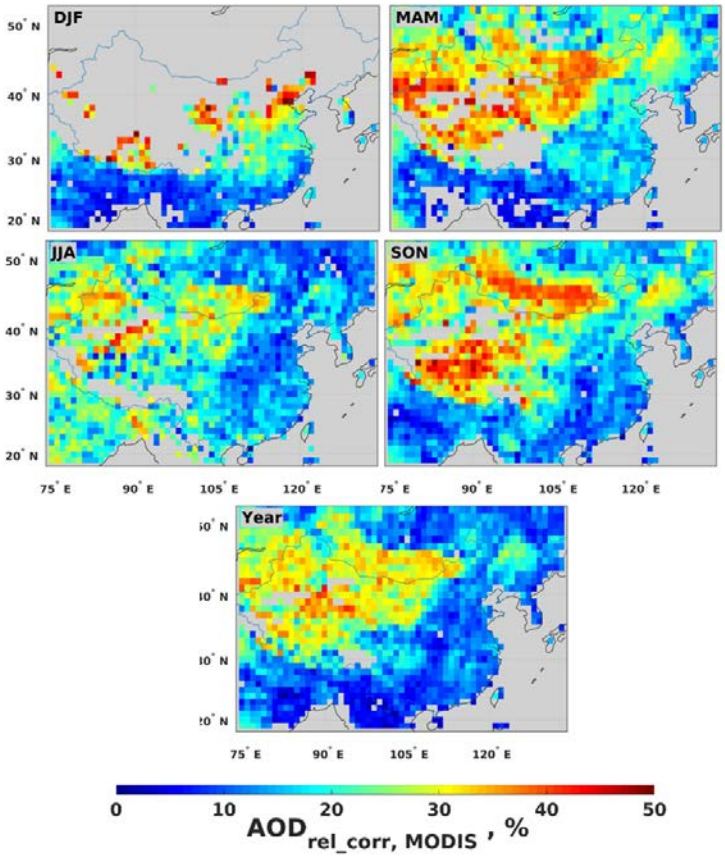


**Figure 3. AOD relative correction for MODIS seasonal (DJF, MAM, JJA, SON) and annual (Year) AOD for the combined AOD dataset obtained with the method introduced in Sect.4.1**

The method was applied pixel-wise to L3 annual and seasonal AOD aggregates from ADV and MODIS to build the yearly and seasonal database of combined AOD. For each season, the AOD relative correction was computed separately, as introduced above for annual AOD.

### 4.2 Results

The time series of the seasonally and annually averaged AOD from ADV (red circles), MODIS (green circles) and combined AOD (yellow rhombs) are shown for all of China and SE of China in Fig.5. Since ADV was negatively biased and MODIS was positively biased with respect to the AERONET AOD, and the biases are similar in absolute value, the combined time series in pre-EOS and post-Envisat periods are practically corrected by increasing ADV and lowering MODIS AOD with the AOD correction as introduced in Sect. 4.1. As expected, the similar interannual variations in the separate datasets are reproduced in the combined time series.

For all seasons, except spring, the difference between ADV and MODIS AOD is small and therefore, the combined time series closely resembles both the ADV and MODIS AOD. In spring, the combined time series show on average lower AOD as compared to MODIS (which, in relative numbers, is about 10-20% lower than the MODIS AOD). However, as for annual aggregates, the interannual variability for seasonal combined AOD is similar for both ADV and MODIS.

The annual and seasonal AOD tendencies for the combined time series are estimated in Sect. 5.

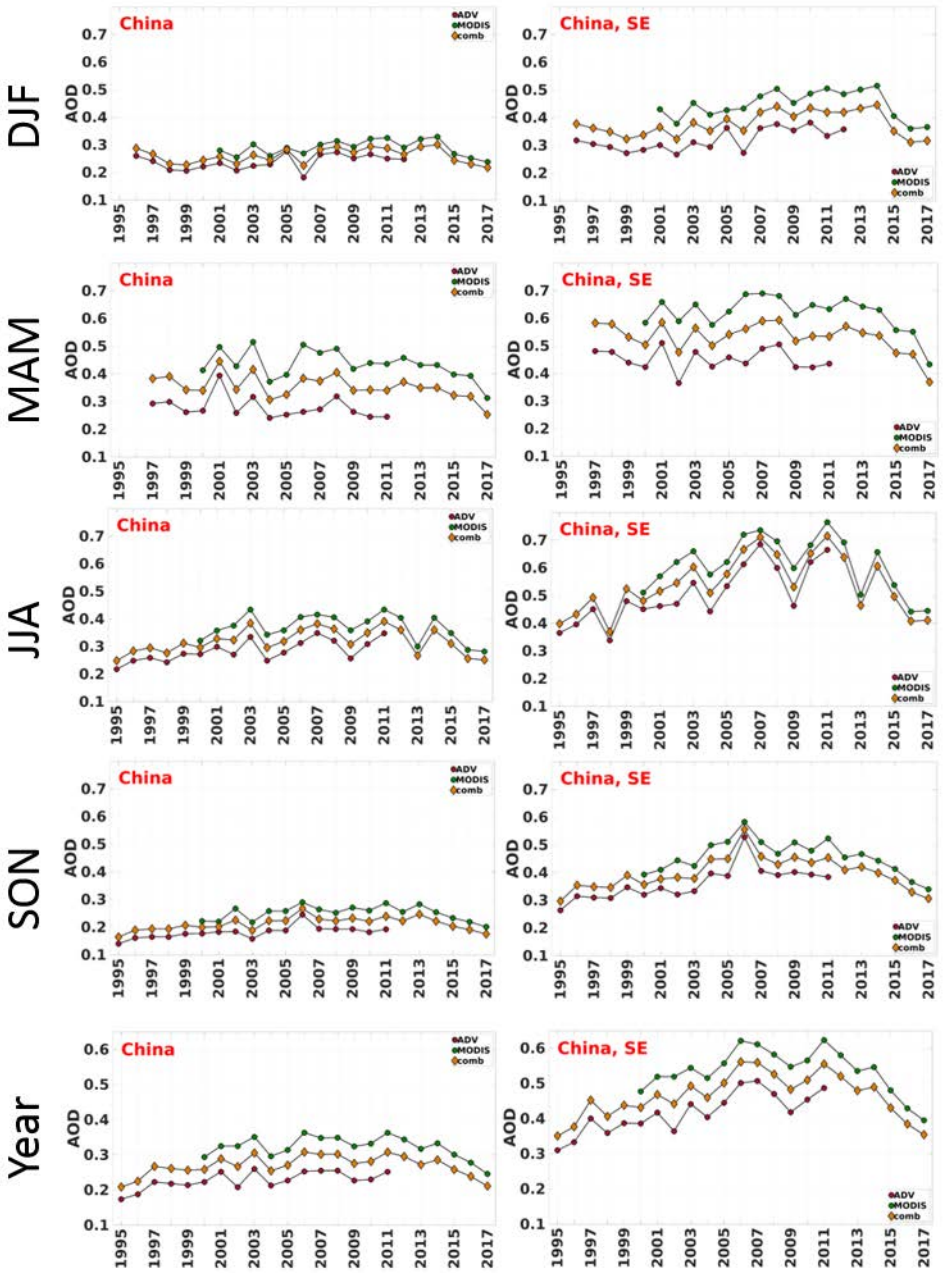


**Figure 4. ADV (red circles), MODIS (green circles) and combined from ADV and MODIS (yellow rhombs) seasonal AOD time series for China (left) and SE China for winter (DJF), spring (MMA), summer (JJA) and autumn (SON) and the whole year. The method used to combine the ADV and MODIS time series is presented in Sect. 4.1.**

### 4.3 Comparison with AERONET

Combined AOD datasets were built from L3 data for seasonal and annual aggregates, thus the comparison with the AERONET is possible for the corresponding periods. We call the current exercise as comparison rather than validation, since the temporal coverage might be different in seasonal and annual aggregates for AERONET, ADV, MODIS, and combined AOD, which might bias the aggregated value. The combined AOD was constructed from three periods (T1-T3, see section 4.1 for details), where different corrections were applied, thus we perform the AOD comparison for the corresponding periods and also for the full ATSR and full MODIS periods. For T1, the number of AERONET locations is limited to perform the comparison (Part 1).

For T2, the agreement between AERONET and combined AOD seasonal and annual aggregates (Fig.5, Table A1) is slightly better than between AERONET and ADV or MODIS separately. R is higher in DJF, JJA and year, 1σ and rms are lower for all seasons and year. For T3 (Table A1), R is considerably higher in spring (0.49 and 0.61 for MODIS and combined, respectively). Bias, slope, 1σ and rms are lower for all seasons for combined AOD compared to MODIS AOD.

For 1998-2012, which covers the period when both AERONET and ADV are available, correlation R is higher for combined AOD in winter, autumn and year; rms is lower in all seasons and year for the combined AOD.

For 2000-2017, which covers the period when both AERONET and MODIS are available, comparison results are similar as in T3.

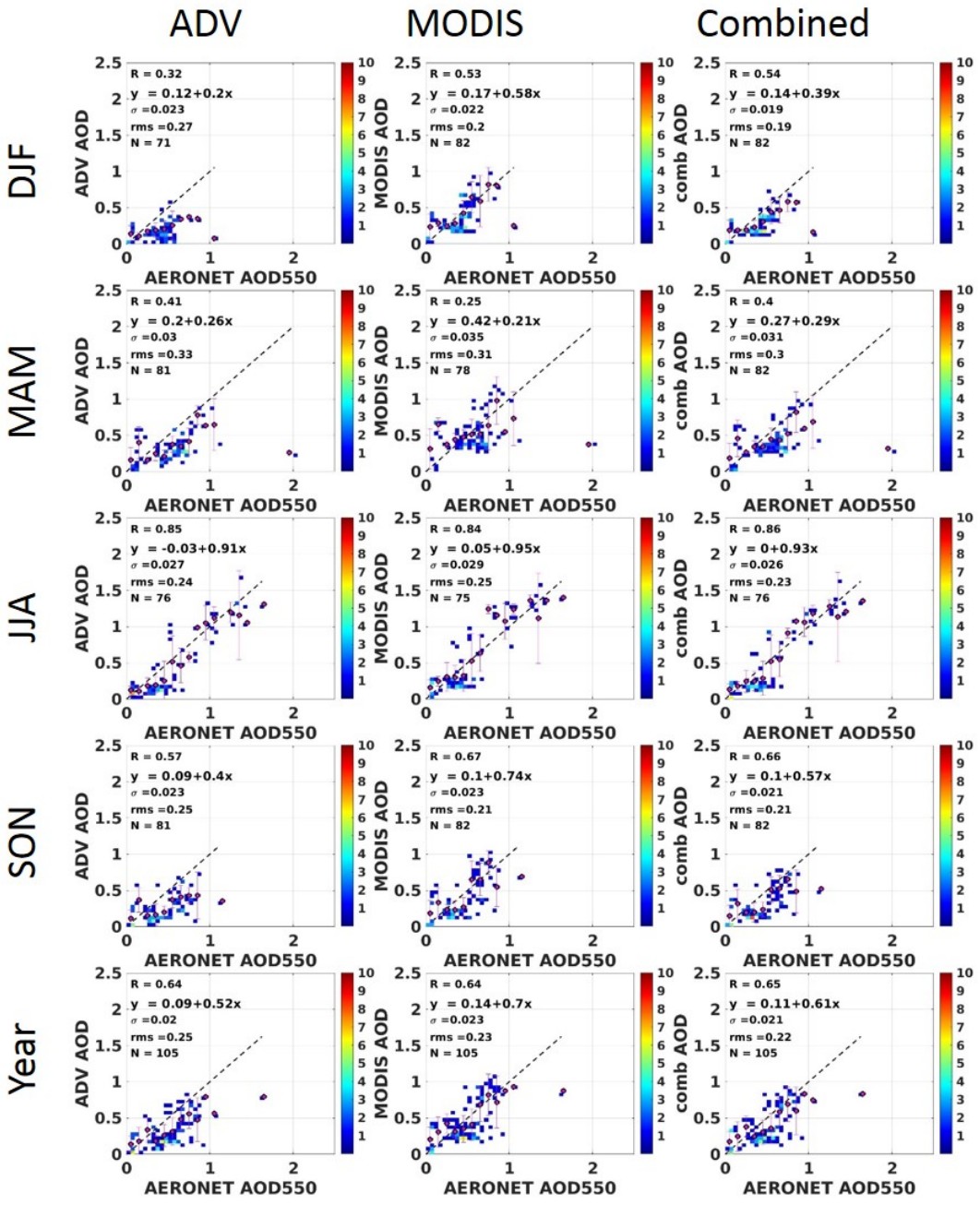


**Figure 5. Density scatterplot of ADV AOD (left), MODIS AOD (middle) and combined AOD (right) versus AOD from AERONET stations over China for the period T2 (2000-2011). The filled circles are the averaged AOD binned in 0.1 AERONET AOD intervals (0.25 for AERONET AOD>1.0) and the vertical lines on each circle represent the 1-σ standard deviation. Statistics in the upper left corner indicate correlation coefficient R, bias, standard deviation, root mean- square error (rms) and the number of data points (N). The colorbar on the right indicates the number of data points in each bin.**

## 5 AOD tendencies for the 1995-2017 period.

### 5.1 Evolution of AOD over China: annual anomaly maps

To study the temporal evolution of the AOD over China during the whole period (WP) from 1995 to 2017, the anomaly maps (Fig. 6) were created by subtracting the multi-year aggregate for the WP from the yearly aggregates. The evolution of the AOD can be followed for different regions and regions with similar or different evolution of the AOD can thus be identified.

Strong negative anomalies over SE China (and the north of India and Bangladesh, which are out of the scope of the current paper) in 1995-2001 show that during that period the AOD was lower compared to the AOD averaged over the WP. Towards 2006, the AOD anomalies were becoming less negative: the yearly AOD was increasing and the anomaly decreased. Starting from 2006, a positive AOD anomaly, which show that the yearly AOD was higher than the AOD averaged over 2000-2011, was observed over SE China. Between 2006 and 2011, the positive anomalies were staying high. Starting from 2011, the anomaly changed from positive to negative, i.e. the AOD decreased. Starting from 2015 the anomaly was mostly negative getting stronger towards 2017, which was the last year in our studies.

The AOD anomaly pattern in SE China was very variable. In the BTH area (region1), the anomaly was strongly negative in 1995, which was the starting years in the time series, and gradually decreased towards 2006, when it turned to positive. In the area over the YRD (region 2) encompassing large urban and industrial developments such as Shanghai and Nanjing, the multi-year average appeared to be quite representative for the AOD with negative anomalies until 2000, after that the anomalies fluctuated around zero with neither very high nor very low values.

Similar AOD behavior was observed in the Sichuan/Chongqing area (region 6) with a strong positive anomaly in 1997 and 1999, followed by negative anomalies in 2000-2002. After 2002, no significant deviations were observed until 2005 when the AOD exceeded the multi-year average and this situation remains, with small fluctuations until 2014 when a strong negative anomaly expanded over the wider region of the SE China during the next (2015-2017) years.

A “belt” of positive AOD anomaly was observed east from the Taklamakan Desert in 2001, which was likely the year of the most intensive dust event during the period of interest. The widespread positive AOD anomaly in 1998 and 2003 in the northeast of China was likely the consequence of the forest fires over Russia.

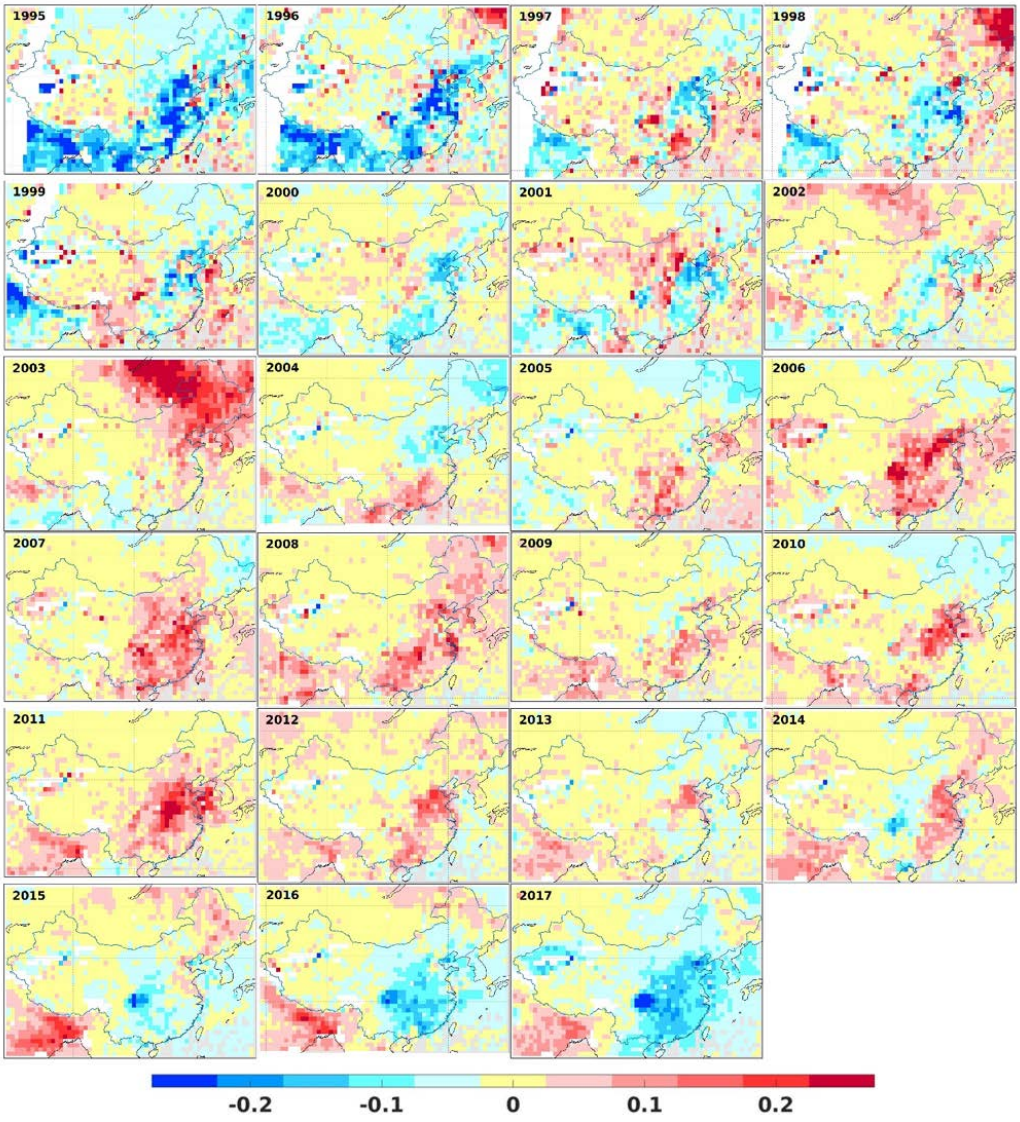


**Figure 6. AOD anomaly maps for the years 1995-2017 calculated for combined AOD. Anomalies were calculated for each year by subtracting the multiyear (1995-2017) average from the annual aggregates.**

Although meteorological conditions play an important role in mixing and transporting pollutants, increasing local aerosol emission from human activities is generally considered as the dominant cause of increasing wintertime haze over China in past decades (Yin et al., 2017). One can isolate meteorological changes from emissions changes by normalizing the aerosol concentrations by aerosol concentration efficiencies (Yang et al., 2018). However, the contribution from wind and its associated languishing patterns explain the historical increase of regional AOD by 10%, while other meteorological contributions show no significant trends over 35 years (Gu et al., 2018).

In the Beijing area, the variation of the AOD is significantly affected by anthropogenic aerosol emissions (Gu et al., 2018) during the last few decades. In the current paper, we aim to show that changes in the AOD follow the emission control policy in China. Below we present a short overview of the emission regulation policies in China during the last two decades.

**5.2 Emissions regulation policies in China during the last two decades.**

Jin et al. (2016) showed that in China: (1) the early policies, until 2005, were ineffective at reducing emissions; (2) during 2006–2012, new instruments, which interact with political incentives, were introduced in the 11th Five-Year Plan. However, emission control policies on air pollution have not been strongly reconsidered in the 11th Five-Year Plan, thus no significant reduction of the air pollution has been observed. Regional air pollution problems dominated by fine particulate matter ($PM_{2.5}$) and ground level ozone ($O_3$) emerged. Nevertheless, the national goal of reducing total sulphur dioxide ($SO_2$) emissions by 10% was achieved (Lin et al., 2010).

Jin et al. (2016) also showed that $SO_2$ emissions, as well as smoke and dust emissions, have been gradually decreasing since 2006. However, the reduction of the total emission of $SO_2$, a single primary pollutant, does not necessarily improve air quality. NOx emissions continued to grow which is explained by the growing number of vehicles mainly in megacities. Total NOx emissions in East China reached their peak levels in 2012, and have stopped increasing since then (van der A et al., 2017), when filtering systems were installed, mainly at power plants but also for heavy industry. These regulations for NOx were announced in 2013 in the Air Pollution Prevention and Control Action Plan (CAAC, 2013).

The "total control" of $SO_2$ and $NO_X$ is strengthened and accelerated in China (Zhang et al., 2017). As an example, the change in standards for cars in 2011–2015 reduces the maximum allowed amount of NOx emissions for on-road vehicles by 50 % (Wu et al., 2017). Further emission control scenarios exist in China to control the entirely coal-burning thermal power plants exists.

The newly designed control policies considered in Wang et al. (2018) are predicted to lead to reductions in January levels in Beijing between −8.6% and −14.8% for $PM_{2.5}$, $PM_{10}$, $NO_2$, and $SO_2$. However, regional differences in emission control exist. More strict regulations for on-road vehicles (e.g. a ban on older polluting cars) were introduced on a city level, e.g. in Beijing, rather than nationwide (van der A et al., 2017).

In June 2013, the State Council issued the Action Plan for Air Pollution Prevention and Control. This document laid out the roadmap for air pollution prevention and control across China for 2013-2017. In 2016, the second report was published (http://cleanairasia.org/wp-content/uploads/2016/08/China-Air-2016-Report-Full.pdf) showing the considerable improvements in emission reduction and air quality. The air quality mostly improved in the developed regions. This report finds that the cities that failed to attain the 2015 air quality target show slow progress and still suffer from poor air quality are concentrated in Henan Province, Shandong Province, and in the northeast of China. These cities had less experience and insufficient capacity in air pollution prevention and control than the more developed regions such as the BTH area. Such regional differences might result in some deviation of regional emission tendencies compared to those averaged over the whole China.

Therefore, three periods, closely related to the Five-Year-Plans (before 2006, 2006-2011, and after 2011), can be identified, when the emission reduction policies in China are reconsidered.

**5.3 AOD seasonal and annual tendencies for the selected periods: 1995-2006 and 2011-2017.**

In addition to selecting the study periods based on emission reduction policy according to the Five-Years Plans, we performed statistical tests, where we looked at the AOD tendencies, uncertainties and errors on annual/seasonal bases for different periods for all selected regions. The results (not shown here) prove that, with some exception (1-2 years shift for a few regions, depending on the season) years 2006 and 2011 can be chosen as a pivot points for the AOD tendencies in China.

Linear regression was applied to individual L3 pixels of the combined AOD time series to estimate the AOD tendencies over China for two periods: 1995-2006 (P1) and 2011-2017 (P2). For P1 and P2, the AOD tendencies (dAOD) per year were estimated, since P2 is too short to estimate the decadal tendencies. Results for 2006-2011 are not shown here since AOD tendency was close to 0.The statistical significance for the tendencies was estimated with the t test (Chandler and Scott, 2011). The results were considered significant at p value<0.05. We also estimated relative tendencies, which are the ratio of tendencies and the corresponding time series averages (Schönwiese and Rapp, 1997). The AOD tendencies and AOD relative tendencies for annual aggregates for P1 and P2 are shown in Figs. 7 and 8, respectively. AOD positive tendencies are denoted by red; AOD negative tendencies are denoted by blue. Pixels for which the tendency is statistically significant are marked in Fig. 7 with green dots.

In P1 (Figs. 7 and 8, left), the AOD increase in summer (JJA) and autumn (SON) with 0.1 to 0.5 (ca. 3-7% of the AOD averaged over the corresponding period) per year contributed most to the annual AOD increase over SE China. In spring (MAM), the AOD tendency was positive over the Yangtze River Delta, northern China and the west of the Tibetan Plateau, (between 0.1 and 0.3, or 2-4%, per year) and negative over the other parts of China. In winter (DJF), when the coverage of the satellite data is lower compared to other seasons (Part 1), irregular patterns of both positive and negative AOD tendencies are observed over China.

For annual aggregates, a statistically significant increase in the AOD of 0.02 to 0.04 (3-6%) per year (Fig. 8, left panel), was observed in P1 over SE China. A similar increase of the AOD was observed over the Taklamakan Desert. However, since the annual AOD over the Taklamakan Desert is lower compared to the SE China (Fig. 10 in Part 1), the relative tendency over the Taklamakan Desert is higher (up to 10% per year for certain pixels) than over SE China for annual AOD. Note that for only few pixels over the Taklamakan Desert the linear fit provides statistically significant results. Over western China, the AOD tendencies were slightly negative (between 0 and -0.01 per year). Over northern China they were slightly positive (between 0 and 0.4 per year) for most pixels. However, the results are not statistically significant since p value is larger than 0.05 almost everywhere in those regions.

In P2 (Figs. 7 and 8, right), the AOD tendencies were opposite in sign, compared to P1. The strongest AOD decrease (up to -0.16 per year) was observed over the northern part of SE China in summer. AOD decrease was slightly lower for other seasons over SE China, while for central and western China the AOD tendencies were close to zero in P2. The relative AOD tendency was between -5% and -10% per year in winter and spring over SE China and more than -15% per year over the Sichuan region in summer and autumn. For annual AOD aggregates, a statistically significant decrease in AOD of -0.02 to -0.04 per year (Fig. 7, right), with an average reduction of 30%-50% between 2011 and 2017, was observed in P2 over SE China. In the Sichuan and Henan regions the AOD decrease more with -0.1 per year. The most negative AOD tendency (ca. -15% per year) is observed in northern China over

the east of Inner Mongolia area (Fig. 8, right). A small AOD decrease is observed over the Taklamakan Desert; a small AOD increase was observed over the most NE part of China. Over other areas, the AOD tendencies in P2 were close to zero.

The low significance of the tendencies can be explained by the low coverage (mostly in winter and spring over snow-covered areas, Part 1), short length of the periods considered and large interannual variations. To reveal more detailed differences in AOD tendencies over China, we apply similar fitting to annual and seasonal AOD averaged over the selected regions in China. The results are presented and discussed in Sect. 5.4.

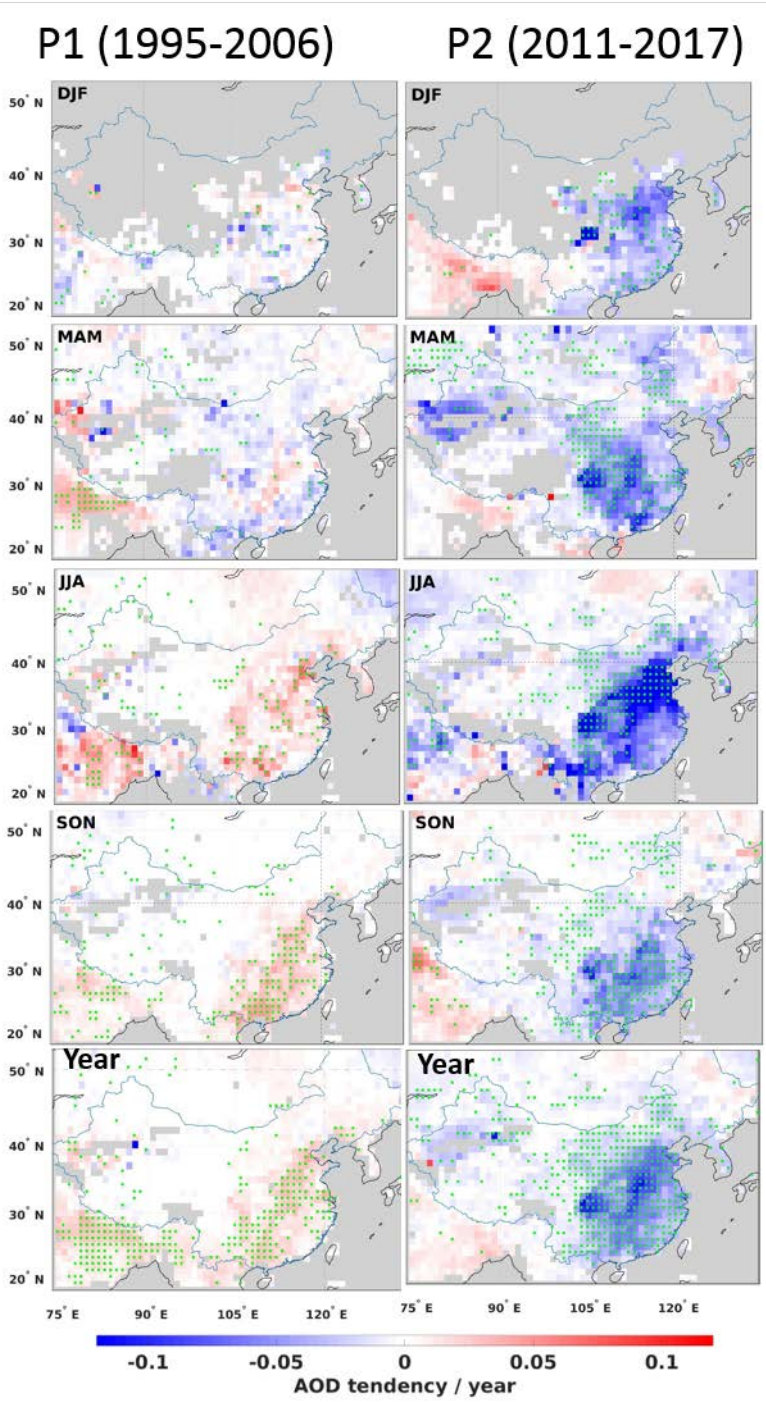


**Figure 7. AOD tendencies (per year, see colorbar) from seasonally and annually aggregated combined AOD time series for two periods: 1995-2006 (P1) and 2011-2017 (P2). Individual pixels are marked with a green dot when the tendency is statistically significant according to the student t test (p value<0.05).**

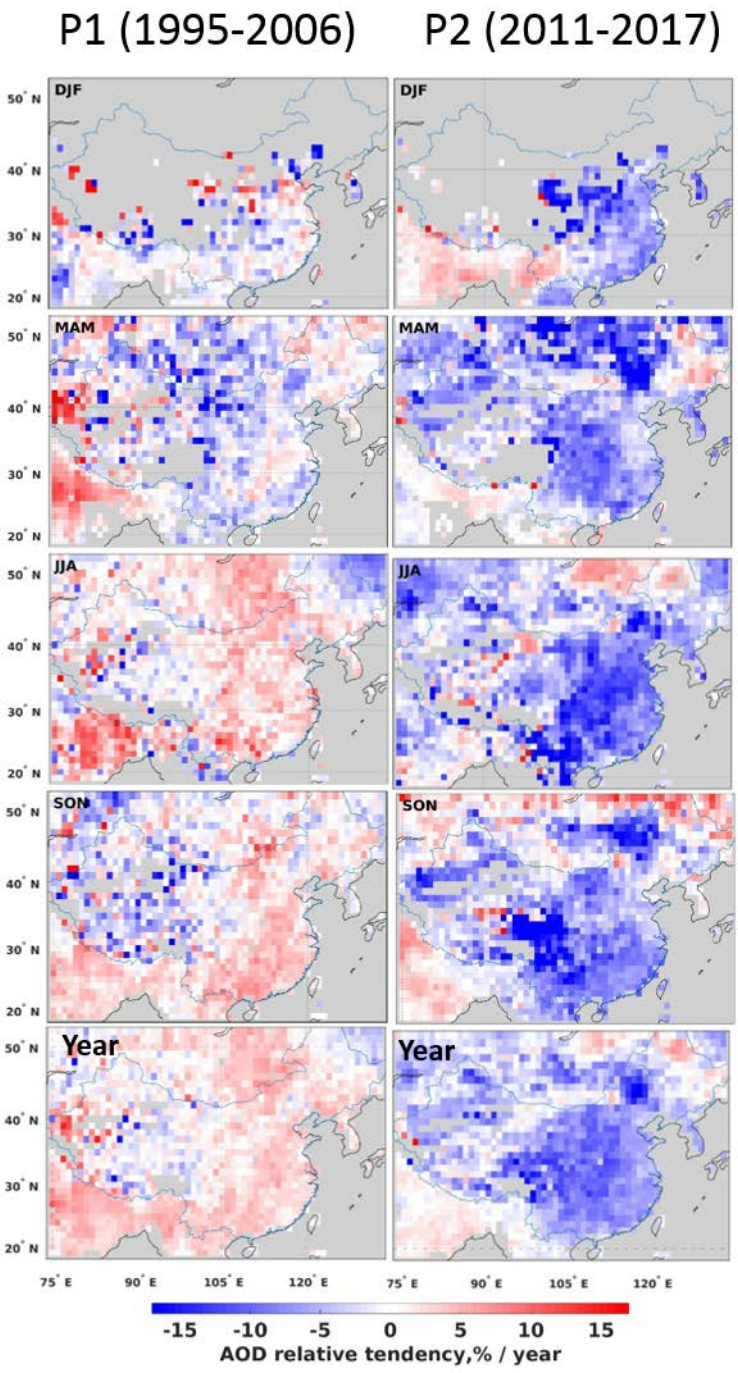


**Figure 8. AOD relative tendencies (per year, see colorbar) from seasonally and annually aggregated combined AOD time series for two periods: 1995-2006 (P1) and 2011-2017 (P2).**

### 5.4 AOD tendencies for the selected regions

#### 5.4.1 Annual AOD tendencies

In Figure 9 we show the annual AOD combined time series (black line) for China, SE China and the 10 selected regions (corresponding red numbers in the left upper corner for each region), which are defined in Sect. 2. For P1 and P2, we also show the AOD tendencies per year and the corresponding relative AOD tendencies. The AOD tendencies and the metrics describing the linear fit for P1 and P2 are summarised in Appendix, Table A2.

For both periods, the tendencies are statistically significant, except for regions 8-10, where, as discussed in Part 1 (Table S1), ADV has low coverage and MODIS has difficulties in retrieving AOD over bright surfaces.

As expected, the AOD tendencies and AOD relative tendencies were positive in P1 in all chosen regions, except for the sparsely populated Tibetan Plateau (region 8), where AOD is very low and varies very little from year to year. The maximum AOD increase in P1 (0.020, or 4%, per year) was observed in the Shanghai area (region 2) and the PRD and Guangxi province (region 7). In the BTH (region 1), and Hunan and Guizhou (region 4), dAOD was also high (0.016, or 3%, per year). Those regions strongly contributed to the AOD increase in SE China (0.014, or 3%, per year). In regions 1, 2, 4, 7 and for all China, uncertainties of the AOD tendencies were within 25% of the AOD tendency in P1. For regions 3, 5, 6 and SE China, the uncertainties related to the tendency estimation were between 25% and 50% of the AOD tendency. In regions 8-10, the uncertainties were higher, which can be explained by the low AOD and lower AOD coverage.

In P2, the AOD decrease was observed in all selected regions and thus also in SE China and all of China. In absolute numbers, dAOD was almost twice higher in P2 than in P1. The most rapid AOD decrease (ca. -0.045, or -8%, per year) was observed in central regions of SE China (regions 4 and 6), while for the rest of SE China, including regions 1, 2, 3, 5 and 7, dAOD was about -0.03, or ca -6%, per year. For regions 8-10, which are less populated and less industrialized, the dAOD was lower (-0.002, -0.014 and -0.004, respectively, or -2%, -5% and -1% per year). Uncertainties related to the AOD tendency estimation were within 25% of the AOD tendency in regions 1 to 7, SE China and China. In regions 8 and 10, the uncertainties were above 50%.

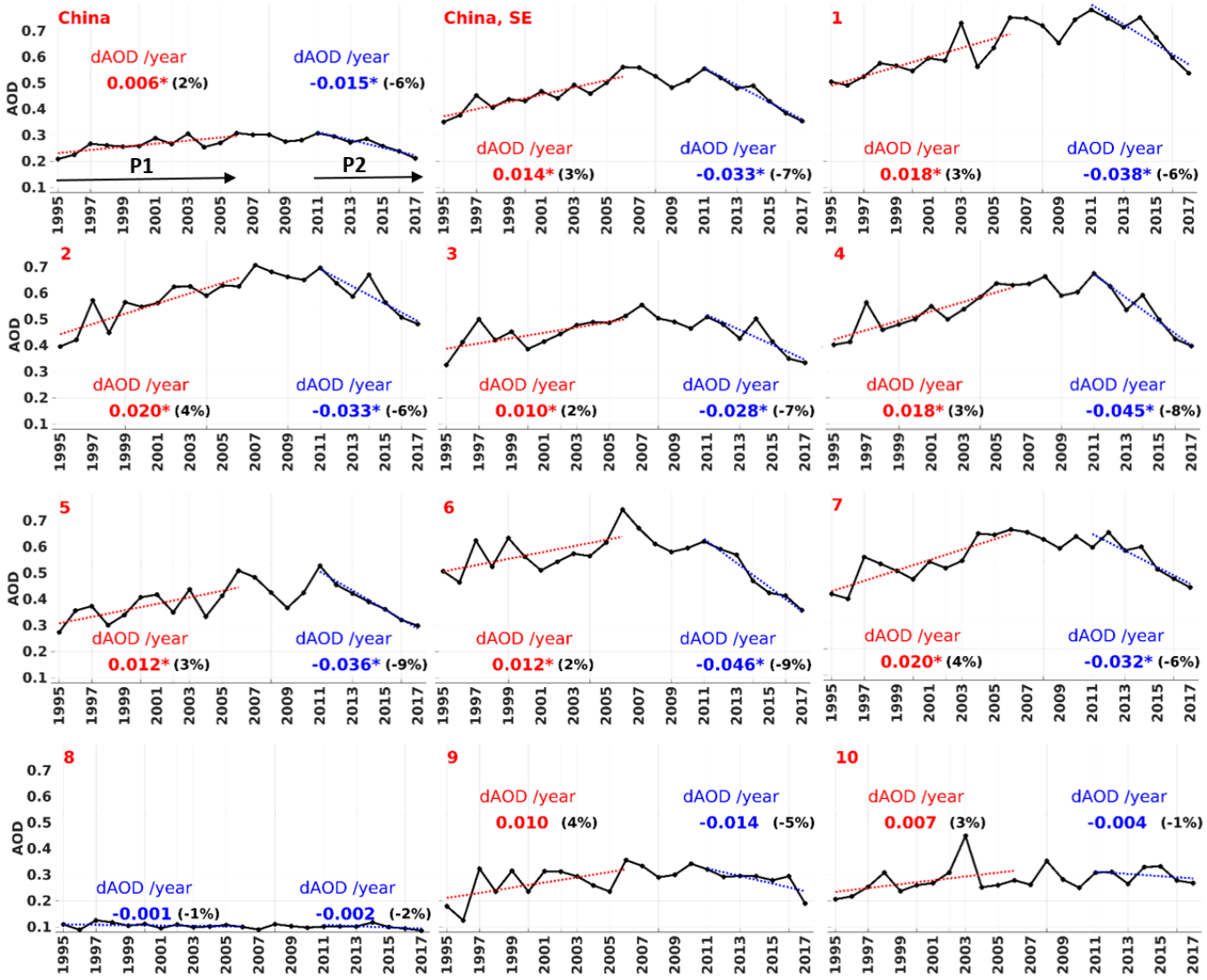


**Figure 9. Time series (black line) of the annually averaged AOD combined from ATSR and MODIS for China, SE China and 10 selected regions (see Fig. 2, corresponding red numbers in the left upper corner for each region). Results for linear fitting of AOD are shown for two periods, P1 (1995-2011) and P2 (2011-2017), marked with black arrows in upper left subplot. Fitting lines (dashed lines) and AOD tendencies (numbers) are shown in red, when AOD tendency was positive and in blue, when AOD tendency was negative; * shows whether the tendency is statistically significant. The corresponding relative AOD tendencies for each fit are shown in brackets (in black, %).**

### 5.4.2 Seasonal AOD tendencies

As shown in Part 1 and Sect 5.3.2, spatial and temporal patterns in the seasonal AOD differ from that of the annual AOD. To examine if the AOD tendencies in different seasons equally contributed to variations of the annual AOD or if the AOD year-to-year

variations are more pronounced in certain seasons, we applied similar regression analysis for the seasonal aggregates of AOD for P1 and P2. As for the annually averaged AOD (Fig. 9), Fig. 10 shows the seasonally combined AOD time series for China, SE China and the 10 selected regions. We also show the linear fitting of AOD for two periods, P1 and P2. For P1 and P2, we show the AOD tendency per year and the corresponding relative AOD tendencies. Time series, linear fitting line and the AOD tendency are shown in different colours for each season.

In P1, during winter and spring, AOD does not vary much (within ±0.01 per year) in any of the regions (Fig.10). A negative AOD tendency of -0.017, or -3%, per year was observed in the Sichuan area (region 6) and in regions 9 and 10, where AOD coverage is low in winter and high AOD variability is observed. In the Hunan and Guizhou Provinces and PRD areas (regions 4 and 7) the AOD decreases a little by ca -0.006 (-2%), per year. In other regions it increases somewhat (ca 1-2% per year). In spring, dAOD was slightly positive in regions 4, 8 and 10 and slightly negative in other regions. In summer and autumn, the AOD increase was discovered in all regions in eastern China (regions 1 to 7). In regions 1, 2, 5 and 6 (north and west of the SE China region, respectively) the AOD increased stronger in summer (ca 0.020, or 3-4%, per year). In regions 3, 4 and 7 (central east to southern part of SE China region) dAOD was larger in autumn, increasing towards south and reaching maxima (0.032, or 6%, per year) in region 7. Over the whole of SE China, dAOD was 0.020, or 4%, per year in summer and 0.016, or 4%, per year in autumn, while in winter and spring dAOD was close to zero. In western and northern China (regions 8-10), year-to-year changes in the seasonal AOD in P1 were low (within ±0.01 per year). Over all China, AOD showed an increase of 0.008, or 2%, and 0.006, or 3%, per year in summer and autumn, respectively, and a small decrease (ca. -0.02, or -1%, per year) in winter and spring. Therefore, summer and spring contribute most to the annual AOD increase (Fig. 7) during the years 1995-2006 (P1) and AOD changes were considerably higher in SE China than in other areas. Note, that the p value for linear fit applied here was often larger than 0.05 (Appendix, Table A3) and the results were thus not statistically significant. However, similar AOD tendencies in neighboring regions (with similar population density and economic activity and meteorological conditions) allow making the overall conclusions.

In SE China, which includes regions 1-7, a strong AOD increase (0.020, or 4%, per year) was observed in summer. The second maxima occurs in autumn (0.016, or 4%, per year). In winter, AOD increase was small (0.001 per year), while in spring a small AOD decrease (-0.003, or -1%, per year) was observed. AOD tendencies averaged seasonally over all of China for P1 show similar AOD increase in summer (0.008, or 2%, per year) and autumn (0.006, or 3%, per year). In winter and spring, AOD decreased slightly (by - 1% per year). AOD tendencies uncertainties were smaller than 50% of the AOD tendencies in regions 2-7, SE China and China in JJA and SON. In other seasons and regions, the uncertainties were >50% of the AOD tendencies.

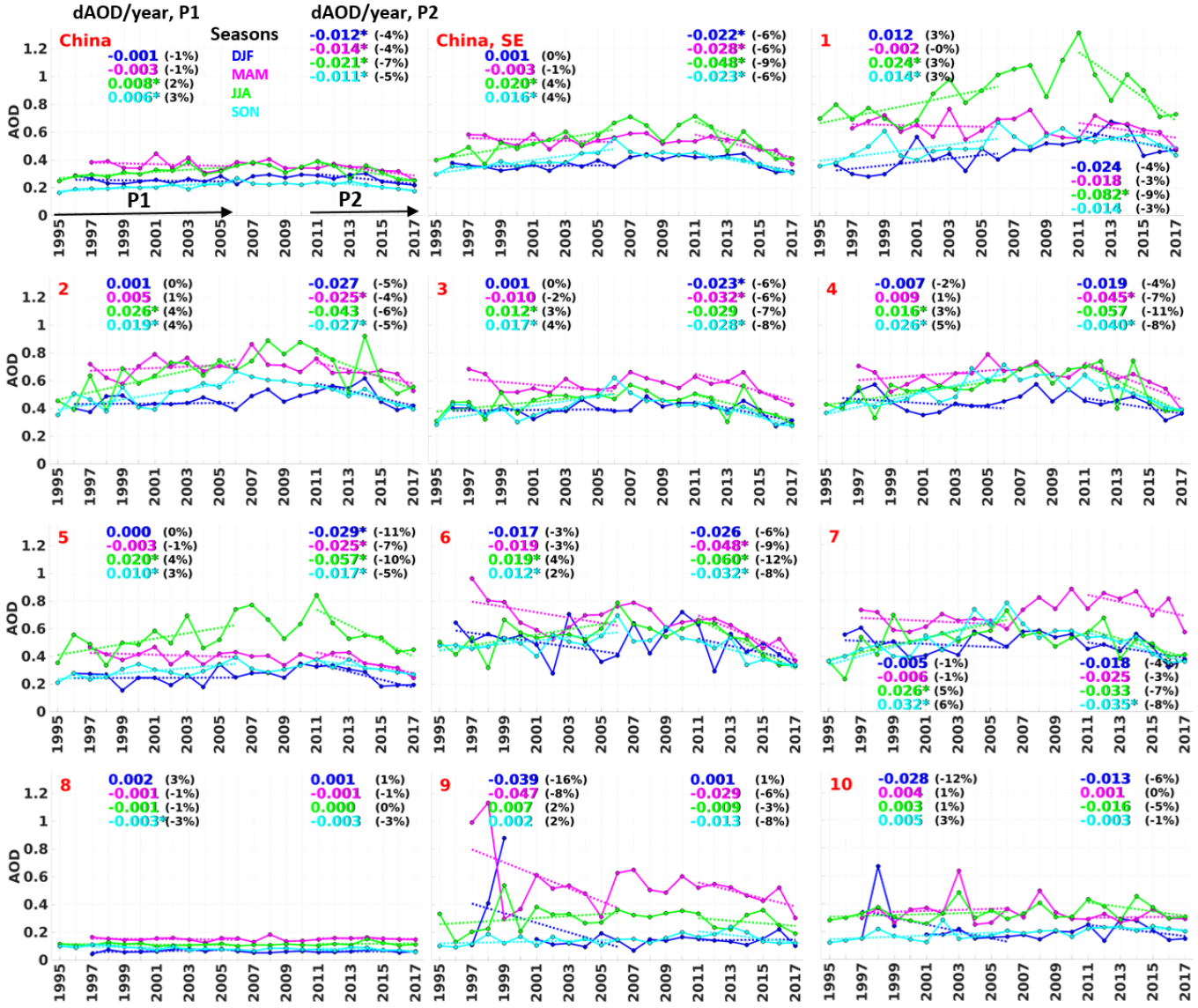


**Figure 10. AOD seasonal long-time series (solid lines), linear fitting (dashed lines) and AOD tendency (numbers) for P1 (1995-2011) and P2 (2011-2017) are shown in different colours for each season (blue for DJF, winter; purple for MAM, spring; green for JJA, summer; and light blue for SOA, autumn) ; * shows whether the tendency is statistically significant. The corresponding relative AOD tendencies for each fit are shown in brackets (in black, %).**

In P2, the AOD tendencies over selected regions were negative and about twice stronger (in absolute numbers) than in P1. AOD tendencies uncertainties were lower in P2 than in P1. However in regions 8-10, the AOD tendencies uncertainties were >50% of the AOD tendencies in all seasons. In winter, the AOD decrease was high (between -0.024 and -0.029 per year) in regions 1, 2, 5. The relative AOD tendency was -11% per year in region 5, which is west of the BTH area, between -4% and -6% per year over SE

China and regions 1-7, and lower over other areas. In spring, the AOD decreased stronger than in winter in regions 3, 4, 6 and 9. A high negative relative tendency (from -6% to -9%) was observed in regions 4-9 in spring. In summer, a high negative AOD relative tendency (between -10% and -12%) was observed in the southern part of SE China, regions 4-7. The highest absolute AOD decrease (-0.082, or -9%, per year) was observed in summer in the BTH area (region 1). In autumn, the AOD tendencies were lower than in spring and summer in most of the regions. In SE China, which includes regions 1-7, the strongest AOD decrease (-0.048, or -9%, per year) was observed in summer. For other seasons, AOD was decreasing by -0.022, -0.028 and -0.023 per year (for DJF, MAM, SON, respectively), which is ca. -6% of the AOD per year for each season.

Over all of China, the AOD decrease was also more pronounced in summer (-0.021, or -7%, per year). For other seasons, AOD was decreasing by -0.012, -0.014 and -0.011 per year (for DJF, MAM, SON, respectively), which is -4% per year in winter and spring and -5% per year in autumn.

Thus, the AOD changes in P2 in summer contribute most to the AOD annual year-to-year variability. AOD seasonal year-to-year changes are more pronounced over eastern China, which is explained by the uneven regional economic development in China.

## 6. Summary and conclusions

With the rapid economic development and further urbanization, the concentration of anthropogenic aerosols have been increasing in China. However, the emission reduction policies in China during the last two decades have successfully reduced the concentration of the atmospheric trace gases (van der A et al., 2017) strengthening the emission control after 2011 (Jin et al., 2016). Here we investigate whether tendencies in the AOD during the last two decades follow up the pollution control policies in China.

The limited lifetime of satellites makes it impossible to follow the AOD changes during several decades with the single instrument. In this paper, we introduced a method to construct a multi-decadal AOD time series by combining data from three different sensors: AATSR-2, ATSR and MODIS/Terra, which together cover the period from 1995 to 2017. The method is based on the ADV and MODIS comparison discussed in Part 1. In brief, (1) ADV and MODIS show similar AOD annual and seasonal spatial and temporal patterns and (2) using AERONET AOD as independent reference data set, ADV is negatively biased, while MODIS is positively biased by about the same amount. The method was applied pixel-wise to L3 annual and seasonal AOD aggregates from ADV and MODIS to construct the combined AOD data set.

This combined data set was used to produce long-term (1995-2017) annual and seasonal AOD time series for all China, SE China and 10 selected regions. Linear regression was applied to individual L3 (1°x1°) pixels of the annual and seasonal combined AOD time series to estimate the changes in AOD over China for two periods: 1995-2006 (P1) and 2011-2017 (P2). Years 2006 and 2011 were identified as pivot points using a statistical analysis. These pivot points coincide which implementation of the Chinese Five-Years Plans. The length of the periods is too short to estimate AOD trends. Therefore, we discuss AOD tendencies.

The main results and conclusions are summarised below:

- In P1, associated with the increase of emissions induced by rapid economic development (Jin et al., 2016), AOD increased strongly over the wide industrial areas. For the annual AOD, the positive tendency of 0.006 (or 2% of the AOD averaged

over the corresponding period), per year was observed for all of China. . In SE China, the annual AOD positive tendency in 1995-2006 was 0.014, or 3%, per year, reaching maxima (0.020, or 4%, per year) in Shanghai and the Pearl River Delta regions.

- Negative AOD tendencies (-0.015, or -6%, per year) were identified across most of China after 2011 in conjunction with effective emission reduction in anthropogenic primary aerosols, $SO_2$ and NOx (Jin et al., 2016; van der A et al., 2017). The air quality mostly improved at the developed regions. Overall, AOD decrease in P2 was 2-3 times stronger than AOD increase in P1 over most of the SE China. The strongest AOD decrease in P2 is observed in the Chengdu (-0.045, or -8%, per year) and Zhengzhou (-0.046, or -9%, per year) areas, while over the North China plane and coastal areas the AOD decrease was <-0.03, or ca -6% per year. In the less populated areas, the AOD decrease was small.
- Seasonal patterns in the AOD regional long-term tendencies are evident. The contribution of seasonal AOD tendencies to annual tendencies was not equal along the year. While the annual AOD tendency was positive in P1, the AOD tendencies in winter and spring were slightly negative (ca. -0.002, or -1%, per year) over most of China during that period. AOD tendencies were positive in summer (0.008, or 2%, per year) and autumn (0.006, or 6%, per year) over all mainland China and SE China (0.020, or 4%, per year and 0.016, or 4%, per year in summer and autumn, respectively). As in P1, the AOD negative tendencies in P2 were higher compared to other seasons in summer over China (ca. -0.021, or -7%, per year) and over SE China (ca. -0.048, or -9%, per year). In the east, seasonal variations in AOD tendencies were less pronounced.

Thus, in the current study the effect of the changes in the emission regulations policy in China is evident in the AOD decrease after 2011. The effect is more visible in the highly populated and industrialized regions in SE China.

**Data availability**

The ATSR data used in this manuscript are publicly available (after registration a password will be issued) at: http://www.icare.univ-lille1.fr/. MODIS data are publicly available at: https://ladsweb.modaps.eosdis.nasa.gov/. AERONET data are available at AERONET: https://aeronet.gsfc.nasa.gov/

**Acknowledgements**:

Work presented in this contribution was undertaken as part of the MarcoPolo project supported by the EU, FP7 SPACE Grant agreement no. 606953 and as part of the Globemission project ESA-ESRIN Data Users Element (DUE), project AO/1-6721/11/I-NB, and contributes to the ESA/MOST DRAGON4 program. The ATSR algorithm (ADV/ASV) used in this work is improved with support from ESA as part of the Climate Change Initiative (CCI) project Aerosol_cci (ESA-ESRIN projects AO/1-6207/09/I-LG and ESRIN/400010987 4/14/1-NB). Further support was received from the Centre of Excellence in Atmospheric Science funded by the Finnish Academy of Sciences Excellence (project no. 272041). Many thanks are expressed to NASA Goddard Space Flight Center (GSFC) Level 1 and Atmosphere Archive and Distribution System (LAADS) (http://ladsweb.nascom.nasa.gov) for making

available the L3 MODIS/Terra C6.1 aerosol data. The AERONET team is acknowledged for establishing and maintaining the AERONET sites used in this study.

**References**

Bouarar, I., Wang, X., and Brasseur, G. P.: Air Pollution in Eastern Asia: An Integrated Perspective, Springer, 504 p., 2017.

CAAC: Clean Air Alliance of China, State Council air pollution prevention and control action plan, issue II, October 2013, available at: http://en.cleanairchina.org/product/6346.html (English translation), (last access: 8 March 2017), 2013.

Cao, Q., Liang, Y., and Niu, X.: China's Air Quality and Respiratory Disease Mortality Based on the Spatial Panel Model., Int. J. of Env. Research and Public Health, 14(9), 1081. http://doi.org/10.3390/ijerph14091081, 2017.

Center for International Earth Science Information Network - CIESIN - Columbia University. Gridded Population of the World, Version 4 (GPWv4): Population Density, Revision 10. Palisades, NY: NASA Socioeconomic Data and Applications Center (SEDAC), https://doi.org/10.7927/H4DZ068D, 2017. Accessed 09.02.2018.

Chan, K. W.: Migration and development in China: trends, geography and current issues, Migration and Development, 1:2, 187-205, 2012.

Chandler, R. and Scott, M.: Statistical methods for trend detection and analysis in the environmental sciences, Wiley, 368, 2011.

de Leeuw, G., Sogacheva, L., Rodriguez, E., Kourtidis, K., Georgoulias, A. K., Alexandri, G., Amiridis, V., Proestakis, E., Marinou, E., Xue, Y., and van der A, R.: Two decades of satellite observations of AOD over mainland China using ATSR-2, AATSR and MODIS/Terra: data set evaluation and large-scale patterns, Atmos. Chem. Phys., 18, 1573-1592, https://doi.org/10.5194/acp-18-1573-2018, 2018.

de Leeuw, G., Holzer-Popp, T., Bevan, S., Davies, W., Descloitres, J., Grainger, R.G., Griesfeller, J., Heckel, A., Kinne, S., Klüser, L., Kolmonen, P., Litvinov, P., Martynenko, D., North, P.J.R., Ovigneur, B., Pascal, N., Poulsen, C., Ramon, D., Schulz, M., Siddans, R., Sogacheva, L., Tanré, D., Thomas, G.E., Virtanen, T.H., von Hoyningen Huene, W., Vountas, M., and Pinnock, S.: Evaluation of seven European aerosol optical depth retrieval algorithms for climate analysis, Remote Sensing of Environment 162 295–315, doi:10.1016/j.rse.2013.04.023, 2015.

Flowerdew, R. J., and Haigh, J.: Retrieval of aerosol optical thickness over land using the ATSR-2 dual-look satellite radiometer, Geogr. Res. Let., Vol: 23, Pages: 351-354, ISSN: 0094-8276, 1996.

Fuzzi, S., Baltensperger, U., Carslaw, K., Decesari, S., Denier van der Gon, H., Facchini, M. C., Fowler, D., Koren, I., Langford, B., Lohmann, U., Nemitz, E., Pandis, S., Riipinen, I., Rudich, Y., Schaap, M., Slowik, J. G., Spracklen, D. V., Vignati, E., Wild, M., Williams, M., and Gilardoni, S.: Particulate matter, air quality and climate: lessons learned and future needs, Atmos. Chem. Phys., 15, 8217-8299, https://doi.org/10.5194/acp-15-8217-2015, 2015.

Gu, X., Bao, F., Cheng, T., Chen, H., Wang, Y., and Guo, H.: The impacts of regional transport and meteorological factors on aerosol optical depth over Beijing, 1980-2014, Scientific Reports, 8, 5113, 2018.

Guo, J. P., Zhang, X. Y., Wu, Y. R., Zhaxi, Y., Che, H. Z., La, B., Wang, W., and Li, X. W.: Spatio-temporal variation trends of satellite-based aerosol optical depth in China during 1980–2008, Atmos. Environ., 4537, 6802–6811, 2011.

Guo, J., Wu, Y., and Li, X.: Long term variation trends of aerosol optical depth in China from MODIS and toms, IEEE Int. Geosci. and Remote Sens. Symp., Munich, 3712-3715, doi:10.1109/IGARSS.2012.6350511, 2012.

He, Q., Ming, Z., and Huang, B.: Spatio-temporal variation and impact factors analysis of satellite based aerosol optical depth over China from 2002 to 2015, Atm. Env., 129, 79-90, 2016.

Holben, B. N., Eck, T. F., Slutsker, I., Tanré, D., Buis, J. P., Setzer, A., Vermote, E., Reagan, J.A., Kaufman, Y., Nakajima, T., Lavenu, F. , Jankowiak, I., and Smirnov, A.: AERONET — A federated instrument network and data archive for aerosol characterization, Remote Sens. of Env., 66, 1–16, 1998.

Hsu, N. C., Tsay, S. C., King, M. D. and Herman, J. R.: Aerosol properties over bright-reflecting source regions, IEEE Trans. Geosci. Remote Sens., 42(3), 557-569, doi:10.1109/TGRS.2004.824067, 2004.

Hsu, N. C., Jeong, M.-J., Bettenhausen, C., Sayer, A. M., Hansell, R., Seftor, C. S., Huang, J. and Tsay, S.-C.: Enhanced Deep Blue aerosol retrieval algorithm: The second generation, J. Geophys. Res. Atmos., 118(16), 9296-9315, doi:10.1002/jgrd.50712, 2013.

Jin, Y., Andersson, H., and Zhang, S.: Air Pollution Control Policies in China: A Retrospective and Prospects, Int. J. of Env. Research and Public Health, 13(12), 1219, doi:10.3390/ijerph13121219, 2016.

Kaufman, Y. J., Tanrı, D., Remer, L.A., Vermote, E.F., Chu, A., and Holben, B.N.: Operational remote sensing of tropospheric aerosol over land from EOS moderate resolution imaging spectroradiometer, J. Geophys. Res., 102(D14), 17051, doi:10.1029/96JD03988, 1997.

Kanakidou, M.: Atmospheric Aerosols and Climate Impacts. In Aerosol Science, eds. I. Colbeck and M. Lazaridis, Chapter 8, John Wiley & Sons, Ltd, doi:10.1002/9781118682555, 2014.

Kolmonen, P., Sogacheva, L., Virtanen, T.H., de Leeuw, G. , and Kulmala, M.: The ADV/ASV AATSR aerosol retrieval algorithm: current status and presentation of a full-mission AOD data set, International Journal of Digital Earth, 9:6, 545-561, doi: 10.1080/17538947.2015.1111450, 2016.

Kourtidis, K., Stathopoulos, S., Georgoulias, A. K., Alexandri, G., and Rapsomanikis, S.: A study of the impact of synoptic weather conditions and water vapor on aerosol–cloud relationships over major urban clusters of China, Atmos. Chem. Phys., 15, 10955-10964, https://doi.org/10.5194/acp-15-10955-2015, 2015.

Kulmala, M.: Atmospheric chemistry: China's choking cocktail. Nature, 526, 497–499, doi:10.1038/526497a, 2015.

Levy, R. C., Mattoo, S., Munchak, L. A., Remer, L. A., Sayer, A. M., Patadia, F., and Hsu, N. C.: The Collection 6 MODIS aerosol products over land and ocean, Atmos. Meas. Tech., 6, 2989-3034, doi:10.5194/amt-6-2989-2013, 2013.

Li, J., Zhiwei Han, Z., and Xie, Z.: Model analysis of long-term trends of aerosol concentrations and direct radiative forcings over East Asia, Tellus B: Chem. and Phys.l Meteorology, 65:1, 20410, doi:10.3402/tellusb.v65i0.20410, 2013.

Li, J., Carlson, B. E., Dubovik, O., and Lacis, A. A.: Recent trends in aerosol optical properties derived from AERONET measurements, Atmos. Chem. Phys., 14, 12271-12289, https://doi.org/10.5194/acp-14-12271-2014, 2014.

Li, J., Li, X., Carlson, B. E., Kahn, R. A., Lacis, A., Dubovik, O., and Nakajima, T.: Reducing multisensor satellite monthly mean aerosol optical depth uncertainty: 1. Objective assessment of current AERONET locations, J. Geophys. Res. Atmos., 121, 13,609–13,627, doi:10.1002/2016JD025469, 2016.

Lin, J., Nielsen, C. P., Zhao, Y., Lei, Y., Liu Y., and Mcelroy, B.: Recent Changes in Particulate Air Pollution over China Observed from Space and the Ground: Effectiveness of Emission Control. Environ. Sci. Technol., 44, 7771–7776, 2010.

Lin, X., Wang, Y., Wang, S., and Wang, D.: Spatial differences and driving forces of land urbanization in China, J. of Geographical Sciences, 25(5): 545-558, 2015.

Luo, Y., Zheng, X., Zhao, T., and Chen, J.: A climatology of aerosol optical depth over China from recent 10 years of MODIS remote sensing data, Int. J. Climatol., 34, 863-870, 2014.

Ma, H., and Chen, Z.: Patterns of Interprovincial Migration in China: Evidence from the Sixth Population Census, Population Research 6: 87–99, 2012.

Mehta, M., Singh, R., Singh, A., Singh, N. and Anshumali: Recent global aerosol optical depth variations and trends—a comparative study using MODIS and MISR level 3 datasets, Remote Sens. Environ., 181, 137–50, 2016.

Morrison, W.M.: China's Economic Rise: History, Trends, Challenges, and Implications for the United States, Congressional Research Service 7-5700, RL33534, https://fas.org/sgp/crs/row/RL33534.pdf. Accessed 05.09.2018.

Nzihou, A. and Stanmore, B.R.: The Formation of Aerosols During the Co-combustion of Coal and Biomass Waste Biomass Valor, 6, 947-957, https://doi.org/10.1007/s12649-015-9390-3, 2015.

Popp, T., de Leeuw, G., Bingen, C., Brühl, C., Capelle, V., Chedin, A., Clarisse, L. , Dubovik, O., Grainger, R., Griesfeller, J., Heckel, A., Kinne, S., Klüser, L., Kosmale, M., Kolmonen, P., Lelli, L., Litvinov, P., Mei, L., North, P., Pinnock, S., Povey, A., Robert, C., Schulz, M., Sogacheva, L., Stebel, K., Stein Zweers, D., Thomas, G., Tilstra, L.G., Vandenbussche, S., Veefkind, P., Vountas, M., and Xue, Y.: Development, production and evaluation of aerosol Climate Data Records from European satellite observations (Aerosol_cci), Remote Sens. 2016, 8, 421, doi:10.3390/rs8050421, 2016.

Remer, L. A., Kaufman, Y. J., Tanré, D., Mattoo, S., Chu, D. A., Martins, J. V., Li, R.-R., Ichoku, C., Levy, R. C., Kleidman, R. G., Eck, T. F., Vermote, E. and Holben, B. N.: The MODIS Aerosol Algorithm, Products, and Validation, J. Atmos. Sci., 62(4), 947-973, doi:10.1175/JAS3385.1, 2005.

Salomonson, V. V., Barnes, W. L., Maymon, P. W., Montgomery, H. E., and Ostrow, H.: MODIS: Advanced facility instrument for studies of the Earth as a system, IEEE T. Geosci. Remote, 27, 145-153, 1989.

Sarrafzadeh, M., Wildt, J., Pullinen, I., Springer, M., Kleist, E., Tillmann, R., Schmitt, S. H., Wu, C., Mentel, T. F., Zhao, D., Hastie, D. R., and Kiendler-Scharr, A.: Impact of $NO_x$ and OH on secondary organic aerosol formation from $\beta$-pinene photooxidation, Atmos. Chem. Phys., 16, 11237-11248, https://doi.org/10.5194/acp-16-11237-2016, 2016.

Sayer, A. M., Thomas, G. E., and Grainger, R. G.: A sea surface reflectance model for (A)ATSR, and application to aerosol retrievals, Atmos. Meas. Tech., 3, 813-838, https://doi.org/10.5194/amt-3-813-2010, 2010.

Sayer, A.M., Munchak, L.A., Hsu, N.C., Levy, R.C., Bettenhausen, C., and Jeong, M.-J.: MODIS Collection 6 aerosol products: Comparison between Aqua's e-Deep Blue, Dark Target, and "merged" data sets, and usage recommendations, J. Geophys. Res. Atmos., 119, 13,965–13,989, doi:10.1002/2014JD022453, 2014.

Schönwiese C.D., and Rapp, J.: Climate trend atlas of Europe based on observations 1891-1990. Kluwer Academic Pub., Netherlands, 228, 1997.

Sihto, S.-L., Kulmala, M., Kerminen, V.-M., Dal Maso, M., Petäjä, T., Riipinen, I., Korhonen, H., Arnold, F., Janson, R., Boy, M., Laaksonen, A., and Lehtinen, K. E. J.: Atmospheric sulphuric acid and aerosol formation: implications from atmospheric measurements for nucleation and early growth mechanisms, Atmos. Chem. Phys., 6, 4079-4091, https://doi.org/10.5194/acp-6-4079-2006, 2006.

Sogacheva, L., Kolmonen, P., Virtanen, T. H., Rodriguez, E., Saponaro, G., and de Leeuw, G.: Post-processing to remove residual clouds from aerosol optical depth retrieved using the Advanced Along Track Scanning Radiometer, Atmos. Meas. Tech., 10, 491-505, doi:10.5194/amt-10-491-2017, 2017.

Sogacheva, L., de Leeuw, G., Rodriguez, E., Kolmonen, P., Georgoulias, A. K., Alexandri, G., Kourtidis, K., Proestakis, E., Marinou, E., Amiridis, V., Xue, Y., and van der A, R. J.: Spatial and seasonal variations of aerosols over China from two decades of multi-satellite observations – Part 1: ATSR (1995–2011) and MODIS C6.1 (2000–2017), Atmos. Chem. Phys., 18, 11389-11407, https://doi.org/10.5194/acp-18-11389-2018, 2018.

Stathopoulos, S., Georgoulias, A. K., and Kourtidis, K.: Spaceborne observations of aerosol - cloud relations for cloud systems of different heights, Atmos. Res., 183, 191-201, 2017.

Streets, D. G., Yan, F., Chin, M., Diehl, T., Mahowald, N., Schultz, M., Wild, M., Wu, Y. and Yu, C.: Anthropogenic and natural contributions to regional trends in aerosol optical depth, 1980–2006, J. Geophys. Res., 114, D00D18, 2009.

Su, X., P. Goloub, I. Chiapello, H. Chen, F. Ducos, and Z. Li: Aerosol variability over East Asia as seen by POLDER space-borne sensors, J. Geophys. Res., 115, D24215, doi:10.1029/2010JD014286, 2010.

Tang, X., McLellan, B. C., Snowden, S., Zhang, B., and Höök, M.: Dilemmas for China: Energy, Economy and Environment. Sustainability, 7, 5508-5520, 2015.

Tanré, D., Kaufman, Y. J., Herman, M. and Mattoo, S.: Remote sensing of aerosol properties over oceans using the MODIS/EOS spectral radiances, J. Geophys. Res. Atmos., 102(D14), 16971-16988, doi:10.1029/96JD03437, 1997.

Tie, X. X., Wu, D., and Brasseur, G.: Lung cancer mortality and exposure to atmospheric aerosol particles in Guangzhou, China. Atmos. Environ., 43, 2375–2377, 2009.

Xie, J. X., and Xia, X. A.: Long-term trend in aerosol optical depth from 1980 to 2001 in north China, Particuology, 6, 106–111, 2008.

Yang, L., and Wang, K.-L.: Regional differences of environmental efficiency of China's energy utilization and environmental regulation cost based on provincial panel data and DEA method, Math. Comput. Model, 58, 1074–1083, 2013.

Yang, Y., Wang, H., Smith, S.J., Zhang, R., Lou, S., Qian, Y., Ma, P. L., and Rasch, P. J.: Recent intensification of winter haze in China linked to foreign emissions and meteorology, Scientific Reports, 8, 2107, 2018.

Yin, Z., Wang, H., and Chen, H: Understanding severe winter haze events in the North China Plain in 2014: roles of climate anomalies, Atmos. Chem. Phys., 17, 1641–1651, 2017.

Zhang, Q., Xin, J., Yin, Y., Wang, L., and Wang, Y.: The variations and trends of MODIS C5 & C6 products' errors in the recent decade over the background and urban areas of North China. Remote Sens., 8, 754, doi:10.3390/rs8090754, 2016.

Zhang, J., Reid, J. S., Alfaro-Contreras, R., and Xian, P.: Has China been exporting less particulate air pollution over the past decade?, Geophys. Res. Lett., 44, 2941–2948, doi:10.1002/2017GL072617, 2017.

Zhang, K.: Urbanization and Industrial Development in China. In book: China's Urbanization and Socioeconomic Impact. Tang**,** Z. (Ed.), Springer, 21-35, doi: 10.1007/978-981-10-4831-9_2, 2017.

Zhao, B., Jiang, J. H., Gu, Y., Diner, D., Worden, J., Liou, K.-N., Su, H., Xing, J., Garay, M., and Huang, L.: Decadal-scale trends in regional aerosol particle properties and their linkage to emission changes, Environ. Res. Lett., 12, 054021, doi.org/10.1088/1748-9326/aa6cb2, 2017.

van der A, R. J., Mijling, B., Ding, J., Koukouli, M. E., Liu, F., Li, Q., Mao, H., and Theys, N.: Cleaning up the air: effectiveness of air quality policy for $SO_2$ and $NO_x$ emissions in China, Atmos. Chem. Phys., 17, 1775-1789, https://doi.org/10.5194/acp-17-1775-2017, 2017.

Veefkind, J. P., de Leeuw, G., and Durkee, P. A.: Retrieval of aerosol optical depth over land using two-angle view satellite radiometry during TARFOX, Geophys. Res. Let., 25 (16), 3135-3138, 1998.

Wang, L., Li, P., Yu, S., Mehmood, K., Li, Z., Chang, S., Liu, W., Rosenfeld, D., Flagan R. C., and Seinfeld, J. H.: Predicted impact of thermal power generation emission control measures in the Beijing-Tianjin-Hebei region on air pollution over Beijing, China, Scientific Reports, 8, 934, doi:10.1038/s41598-018-19481-0, 2018.

Wang, P. , Ning, S., Dai, J., Sun, J., Li, M., Song, Q., Dai, X., Zhao, J., and Yu, D.: Trends and Variability in Aerosol Optical Depth over North China from MODIS C6 Aerosol Products during 2001–2016, Atmosphere, 8, 223, doi:10.3390/atmos8110223, 2017.

Weatherhead, E. C., Harder, J., Araujo-Pradere, E. A., Bodeker, G., English, J. M., Flynn, L. E., Frith, S. M., Lazo, J. K., Pilewskie, P., Weber, M., and Woods, T. N.: How long do satellites need to overlap? Evaluation of climate data stability from overlapping satellite records, Atmos. Chem. Phys., 17, 15069-15093, https://doi.org/10.5194/acp-17-15069-2017, 2017.

World Bank: China Economic Update, December 2017, http://pubdocs.worldbank.org/en/485891513640933352/CEU-Dec-1219-EN.pdf. Accessed 06.09.2018.

Wu, Y., Zhang, S., Hao, J., Liu, H., Wu, X., Hu, J., Walsh, M. P., Wallington, T. J., Zhang, K. M., and Stevanovic, S.: On-road vehicle emissions and their control in China: A review and outlook, Sci. Total Environ., 574, 332–349, doi:10.1016/j.scitotenv.2016.09.040, 2017.

## Appendix

**Table A1. Comparison of the seasonal and annual ADV, MODIS and Combined AOD with AERONET AOD for different periods: T2 (2000-2011, ADV and MODIS overlapping period), T3 (2011-2017, MODIS), ADV period (1998-2012), MODIS/Terra whole period (2000-2017); number of points (N), correlation coefficient (R), standard deviation (σ) and root meat square error (rms).**

| season | collection | N | R | slope | bias | σ | rms |
|---|---|---|---|---|---|---|---|
| T2 (2000-2011) | | | | | | | |
| DJF | ADV | 71 | 0,32 | 0,12 | 0,2 | 0,023 | 0,27 |
| | MODIS | 82 | 0,53 | 0,17 | 0,58 | 0,022 | 0,2 |
| | Combined | 82 | 0,54 | 0,14 | 0,39 | 0,019 | 0,19 |
| MAM | ADV | 81 | 0,41 | 0,2 | 0,26 | 0,03 | 0,33 |
| | MODIS | 78 | 0,25 | 0,42 | 0,21 | 0,035 | 0,31 |
| | Combined | 82 | 0,4 | 0,27 | 0,29 | 0,031 | 0,3 |
| JJA | ADV | 76 | 0,85 | -0,03 | 0,91 | 0,027 | 0,24 |
| | MODIS | 75 | 0,84 | 0,05 | 0,95 | 0,029 | 0,25 |
| | Combined | 76 | 0,86 | 0 | 0,93 | 0,026 | 0,23 |
| SON | ADV | 81 | 0,57 | 0,09 | 0,4 | 0,023 | 0,25 |
| | MODIS | 82 | 0,67 | 0,1 | 0,74 | 0,023 | 0,21 |
| | Combined | 82 | 0,66 | 0,1 | 0,57 | 0,021 | 0,21 |
| Year | ADV | 105 | 0,64 | 0,09 | 0,52 | 0,02 | 0,25 |
| | MODIS | 105 | 0,64 | 0,14 | 0,7 | 0,023 | 0,23 |
| | Combined | 105 | 0,65 | 0,11 | 0,61 | 0,021 | 0,22 |
| T3 (2011-2017) | | | | | | | |
| DJF | MODIS | 52 | 0,59 | 0,17 | 0,8 | 0,028 | 0,23 |
| | Combined | 52 | 0,59 | 0,15 | 0,51 | 0,021 | 0,15 |
| MAM | MODIS | 53 | 0,49 | 0,29 | 0,47 | 0,032 | 0,23 |
| | Combined | 58 | 0,61 | 0,17 | 0,5 | 0,027 | 0,21 |
| JJA | MODIS | 49 | 0,93 | 0,03 | 1,09 | 0,021 | 0,16 |
| | Combined | 50 | 0,94 | -0,01 | 1,04 | 0,018 | 0,13 |
| SON | MODIS | 44 | 0,65 | 0,14 | 0,77 | 0,032 | 0,22 |
| | Combined | 44 | 0,64 | 0,12 | 0,59 | 0,028 | 0,18 |
| Year | MODIS | 62 | 0,71 | 0,1 | 0,87 | 0,026 | 0,21 |
| | Combined | 62 | 0,71 | 0,08 | 0,76 | 0,023 | 0,18 |
| ADV period (1998-2012) | | | | | | | |
| DJF | ADV | 72 | 0,33 | 0,12 | 0,2 | 0,023 | 0,27 |
| | Combined | 84 | 0,54 | 0,14 | 0,4 | 0,018 | 0,19 |
| MAM | ADV | 88 | 0,39 | 0,2 | 0,25 | 0,029 | 0,33 |
| | Combined | 89 | 0,38 | 0,28 | 0,28 | 0,029 | 0,3 |
| JJA | ADV | 81 | 0,85 | -0,04 | 0,92 | 0,025 | 0,24 |
| | Combined | 81 | 0,86 | 0 | 0,94 | 0,025 | 0,22 |
| SON | ADV | 85 | 0,57 | 0,09 | 0,41 | 0,022 | 0,25 |
| | Combined | 86 | 0,66 | 0,09 | 0,58 | 0,02 | 0,2 |

| | | | | | | | |
|---|---|---|---|---|---|---|---|
| Year | ADV | 112 | 0,62 | 0,09 | 0,5 | 0,02 | 0,26 |
| | Combined | 112 | 0,63 | 0,11 | 0,59 | 0,02 | 0,23 |
| MODIS period (2000-2017) | | | | | | | |
| DJF | MODIS | 124 | 0,53 | 0,18 | 0,61 | 0,019 | 0,21 |
| | Combined | 124 | 0,53 | 0,15 | 0,4 | 0,015 | 0,18 |
| MAM | MODIS | 125 | 0,31 | 0,38 | 0,27 | 0,026 | 0,29 |
| | Combined | 133 | 0,46 | 0,24 | 0,34 | 0,022 | 0,27 |
| JJA | MODIS | 117 | 0,87 | 0,05 | 0,96 | 0,02 | 0,22 |
| | Combined | 118 | 0,88 | 0,01 | 0,93 | 0,018 | 0,2 |
| SON | MODIS | 117 | 0,65 | 0,12 | 0,73 | 0,02 | 0,22 |
| | Combined | 117 | 0,65 | 0,1 | 0,57 | 0,018 | 0,2 |
| Year | MODIS | 158 | 0,65 | 0,14 | 0,7 | 0,018 | 0,22 |
| | Combined | 158 | 0,66 | 0,11 | 0,61 | 0,016 | 0,21 |

**Table A2. AOD tendency (dAOD) per year and statistics for the annual combined AOD time series linear fitting (p-value, bias, slope, uncertainty and relative error (re, %)) for two periods: P1 (1995-2006), and P2 (2011-2017) for different regions (r, where region 11 is all mainland China and region 12 is mainland SE China).**

| | P1 | | | | | P2 | | | | |
|---|---|---|---|---|---|---|---|---|---|---|
| r | dAOD, period | unc | p | re, % | dAOD, year | dAOD, period | unc | p | re, % | dAOD, year |
| 1 | 0,198 | 0,051 | 0,002 | 6,8 | 0,018 | -0,229 | 0,037 | 0,003 | 5,6 | -0,038 |
| 2 | 0,215 | 0,046 | 0,001 | 6,7 | 0,020 | -0,199 | 0,041 | 0,008 | 7,2 | -0,033 |
| 3 | 0,113 | 0,042 | 0,015 | 7,5 | 0,010 | -0,171 | 0,038 | 0,010 | 9,1 | -0,029 |
| 4 | 0,198 | 0,042 | 0,000 | 6,4 | 0,018 | -0,271 | 0,034 | 0,001 | 6,7 | -0,045 |
| 5 | 0,137 | 0,049 | 0,013 | 10,3 | 0,012 | -0,218 | 0,014 | 0,000 | 3,8 | -0,036 |
| 6 | 0,134 | 0,063 | 0,043 | 8,6 | 0,012 | -0,276 | 0,021 | 0,000 | 4,6 | -0,046 |
| 7 | 0,219 | 0,047 | 0,001 | 7,1 | 0,020 | -0,190 | 0,036 | 0,006 | 7,0 | -0,032 |
| 8 | -0,008 | 0,010 | 0,427 | 7,4 | -0,001 | -0,014 | 0,009 | 0,216 | 9,1 | -0,002 |
| 9 | 0,110 | 0,059 | 0,072 | 17,8 | 0,010 | -0,087 | 0,031 | 0,055 | 11,3 | -0,014 |
| 10 | 0,081 | 0,060 | 0,172 | 17,2 | 0,007 | -0,026 | 0,029 | 0,476 | 10,0 | -0,004 |
| 11 | 0,065 | 0,020 | 0,006 | 6,0 | 0,006 | -0,089 | 0,011 | 0,001 | 4,4 | -0,015 |
| 12 | 0,153 | 0,027 | 0,000 | 4,8 | 0,014 | -0,198 | 0,016 | 0,000 | 3,6 | -0,033 |

**Table A3. AOD tendency (dAOD) per year and statistics for linear fitting (p value, bias, slope, uncertainty (unc) and relative error (re, %)) for the seasonally combined AOD time series for two periods: P1 (1995-2006) and P2 (2011-2017) for different regions (r, where region 11 is all mainland China and region 12 is the mainland SE China) and different seasons (s, 1 – winter, 2 – spring, 3 – summer, 4 - autumn).**

| r | s | P1 | | | | | P2 | | | | |
|---|---|---|---|---|---|---|---|---|---|---|---|
| | | dAOD, period | unc | p | re, % | dAOD, year | dAOD, period | unc | p | re, % | dAOD, year |
| 1 | SON | 0,159 | 0,077 | 0,049 | 12,9 | 0,015 | -0,082 | 0,045 | 0,166 | 8,6 | -0,014 |
| 2 | DJF | 0,009 | 0,041 | 0,819 | 7,7 | 0,001 | -0,160 | 0,066 | 0,085 | 13,6 | -0,027 |
| 2 | MAM | 0,046 | 0,064 | 0,493 | 7,9 | 0,005 | -0,150 | 0,045 | 0,034 | 7,2 | -0,025 |
| 2 | JJA | 0,288 | 0,092 | 0,007 | 12,1 | 0,026 | -0,257 | 0,149 | 0,190 | 23,3 | -0,043 |
| 2 | SON | 0,204 | 0,070 | 0,010 | 11,3 | 0,019 | -0,161 | 0,027 | 0,003 | 5,8 | -0,027 |
| 3 | DJF | 0,010 | 0,036 | 0,779 | 7,5 | 0,001 | -0,139 | 0,047 | 0,049 | 13,0 | -0,023 |
| 3 | MAM | -0,087 | 0,056 | 0,153 | 8,4 | -0,010 | -0,189 | 0,054 | 0,028 | 10,1 | -0,032 |
| 3 | JJA | 0,127 | 0,058 | 0,039 | 10,5 | 0,012 | -0,176 | 0,093 | 0,157 | 23,9 | -0,029 |
| 3 | SON | 0,188 | 0,070 | 0,016 | 13,8 | 0,017 | -0,168 | 0,032 | 0,005 | 9,1 | -0,028 |
| 4 | DJF | -0,075 | 0,063 | 0,245 | 11,8 | -0,008 | -0,113 | 0,048 | 0,093 | 11,8 | -0,019 |
| 4 | MAM | 0,078 | 0,077 | 0,337 | 10,2 | 0,009 | -0,268 | 0,050 | 0,005 | 8,8 | -0,045 |
| 4 | JJA | 0,181 | 0,064 | 0,012 | 9,9 | 0,017 | -0,343 | 0,135 | 0,076 | 27,0 | -0,057 |
| 4 | SON | 0,287 | 0,061 | 0,000 | 9,8 | 0,026 | -0,239 | 0,026 | 0,000 | 5,4 | -0,040 |
| 5 | DJF | 0,004 | 0,056 | 0,947 | 18,6 | 0,000 | -0,173 | 0,031 | 0,004 | 12,9 | -0,029 |
| 5 | MAM | -0,030 | 0,046 | 0,530 | 9,6 | -0,003 | -0,151 | 0,038 | 0,017 | 11,2 | -0,025 |
| 5 | JJA | 0,216 | 0,099 | 0,040 | 15,3 | 0,020 | -0,341 | 0,072 | 0,009 | 13,6 | -0,057 |
| 5 | SON | 0,111 | 0,038 | 0,010 | 10,5 | 0,010 | -0,102 | 0,024 | 0,013 | 7,6 | -0,017 |
| 6 | DJF | -0,167 | 0,114 | 0,161 | 18,8 | -0,017 | -0,156 | 0,118 | 0,298 | 27,3 | -0,026 |
| 6 | MAM | -0,174 | 0,120 | 0,182 | 14,6 | -0,019 | -0,288 | 0,047 | 0,003 | 9,0 | -0,048 |
| 6 | JJA | 0,213 | 0,098 | 0,039 | 14,2 | 0,019 | -0,358 | 0,032 | 0,000 | 7,2 | -0,060 |
| 6 | SON | 0,129 | 0,062 | 0,047 | 9,6 | 0,012 | -0,194 | 0,054 | 0,024 | 13,5 | -0,032 |
| 7 | DJF | -0,053 | 0,074 | 0,471 | 12,4 | -0,005 | -0,111 | 0,072 | 0,232 | 16,8 | -0,019 |
| 7 | MAM | -0,051 | 0,057 | 0,395 | 7,5 | -0,006 | -0,151 | 0,098 | 0,231 | 13,1 | -0,025 |
| 7 | JJA | 0,287 | 0,102 | 0,012 | 16,0 | 0,026 | -0,197 | 0,087 | 0,103 | 18,6 | -0,033 |
| 7 | SON | 0,353 | 0,079 | 0,001 | 12,8 | 0,032 | -0,209 | 0,043 | 0,008 | 9,7 | -0,035 |
| 8 | DJF | 0,018 | 0,011 | 0,123 | 14,0 | 0,002 | 0,004 | 0,008 | 0,657 | 12,7 | 0,001 |
| 8 | MAM | -0,007 | 0,012 | 0,551 | 6,7 | -0,001 | -0,005 | 0,006 | 0,505 | 4,1 | -0,001 |
| 8 | JJA | -0,008 | 0,009 | 0,377 | 6,3 | -0,001 | 0,003 | 0,018 | 0,888 | 15,5 | 0,001 |
| 8 | SON | -0,029 | 0,011 | 0,016 | 10,0 | -0,003 | -0,015 | 0,012 | 0,309 | 16,4 | -0,003 |
| 9 | DJF | -0,312 | 0,247 | 0,251 | 115,3 | -0,039 | 0,005 | 0,043 | 0,917 | 30,1 | 0,001 |
| 9 | MAM | -0,420 | 0,253 | 0,132 | 39,4 | -0,047 | -0,172 | 0,065 | 0,065 | 14,2 | -0,029 |
| 9 | JJA | 0,082 | 0,108 | 0,432 | 28,6 | 0,007 | -0,055 | 0,068 | 0,505 | 25,6 | -0,009 |
| 9 | SON | 0,025 | 0,032 | 0,403 | 18,7 | 0,002 | -0,078 | 0,038 | 0,127 | 23,8 | -0,013 |
| 10 | DJF | -0,223 | 0,157 | 0,200 | 68,3 | -0,028 | -0,080 | 0,066 | 0,337 | 33,6 | -0,013 |
| 10 | MAM | 0,032 | 0,118 | 0,793 | 28,8 | 0,004 | 0,007 | 0,033 | 0,852 | 11,3 | 0,001 |
| 10 | JJA | 0,036 | 0,062 | 0,544 | 15,0 | 0,003 | -0,098 | 0,064 | 0,232 | 18,2 | -0,016 |
| 10 | SON | 0,050 | 0,046 | 0,264 | 21,4 | 0,005 | -0,017 | 0,014 | 0,349 | 6,6 | -0,003 |
| 11 | DJF | -0,013 | 0,023 | 0,556 | 7,4 | -0,001 | -0,071 | 0,023 | 0,041 | 8,9 | -0,012 |
| 11 | MAM | -0,028 | 0,045 | 0,555 | 10,5 | -0,003 | -0,084 | 0,025 | 0,030 | 7,8 | -0,014 |

| | | | | | | | | | | | |
|---|---|---|---|---|---|---|---|---|---|---|---|
| 11 | JJA | 0,083 | 0,026 | 0,006 | 6,6 | 0,008 | -0,125 | 0,039 | 0,036 | 12,9 | -0,021 |
| 11 | SON | 0,065 | 0,016 | 0,001 | 6,1 | 0,006 | -0,064 | 0,013 | 0,007 | 6,1 | -0,011 |
| 12 | DJF | 0,011 | 0,024 | 0,642 | 5,6 | 0,001 | -0,130 | 0,036 | 0,024 | 9,7 | -0,022 |
| 12 | MAM | -0,029 | 0,039 | 0,476 | 6,2 | -0,003 | -0,165 | 0,038 | 0,012 | 7,9 | -0,028 |
| 12 | JJA | 0,217 | 0,048 | 0,001 | 7,5 | 0,020 | -0,288 | 0,066 | 0,012 | 13,2 | -0,048 |
| 12 | SON | 0,175 | 0,036 | 0,000 | 7,4 | 0,016 | -0,140 | 0,015 | 0,000 | 4,0 | -0,023 |